USGS
science for a changing world

Prepared in cooperation with the U.S. Army Corps of Engineers, Chicago District

Uncertainty Analysis of Index-Velocity Meters and Discharge Computations at the Chicago Sanitary and Ship Canal near Lemont, Illinois, Water Years 2006–16

Open-File Report 2022–1007

U.S. Department of the Interior
U.S. Geological Survey

Uncertainty Analysis of Index-Velocity Meters and Discharge Computations at the Chicago Sanitary and Ship Canal near Lemont, Illinois, Water Years 2006–16

By Thomas M. Over, Marian Muste, James J. Duncker, Heng-Wei Tsai, P. Ryan Jackson, Kevin K. Johnson, Frank L. Engel, and Crystal D. Prater

Prepared in cooperation with the U.S. Army Corps of Engineers, Chicago District

Open-File Report 2022–1007

U.S. Geological Survey, Reston, Virginia: 2022

For more information on the USGS—the Federal source for science about the Earth, its natural and living resources, natural hazards, and the environment—visit https://www.usgs.gov or call 1–888–ASK–USGS.

For an overview of USGS information products, including maps, imagery, and publications, visit https://store.usgs.gov/.

Suggested citation:
Over, T.M., Muste, M., Duncker, J.J., Tsai, H., Jackson, P.R., Johnson, K.K., Engel, F.L., and Prater, C.D., 2022, Uncertainty analysis of index-velocity meters and discharge computations at the Chicago Sanitary and Ship Canal near Lemont, Illinois, water years 2006–16: U.S. Geological Survey Open-File Report 2022–1007, 35 p., https://doi.org/10.3133/ofr20221007.

Associated data for this publication:
Prater, C.D., LeRoy, J.Z., Engel, F.L., and Johnson, K.K., 2021, Discharge measurements at U.S. Geological Survey streamgage 05536890 Chicago Sanitary and Ship Canal near Lemont, Illinois, 2005–2013: U.S. Geological Survey data release, https://doi.org/10.5066/F7X63K41.

U.S. Geological Survey, 2021, USGS water data for the Nation: U.S. Geological Survey National Water Information System database, https://doi.org/10.5066/F7P55KJN.

ISSN 2331-1258 (online)

Acknowledgments

The work described in this report was completed in cooperation with the U.S. Army Corps of Engineers, Chicago District. The authors would like to thank Lake Michigan Diversion Accounting project managers Tzuo-Ying Su and Jeff Fuller for their guidance and support.

Contents

Figures

Tables

Conversion Factors

U.S. customary units to International System of Units

Multiply	By	To obtain
	Length	
foot (ft)	0.3048	meter (m)
mile (mi)	1.609	kilometer (km)
	Area	
square foot (ft^2)	929.0	square centimeter (cm^2)
square foot (ft^2)	0.09290	square meter (m^2)
	Flow rate	
foot per second (ft/s)	0.3048	meter per second (m/s)
cubic foot per second (ft^3/s)	0.02832	cubic meter per second (m^3/s)

International System of Units to U.S. customary units

Multiply	By	To obtain
	Length	
meter (m)	3.281	foot (ft)
meter (m)	1.094	yard (yd)

Temperature in degrees Fahrenheit (°F) may be converted to degrees Celsius (°C) as follows:

$$°C = (°F - 32) / 1.8.$$

Datum

Horizontal coordinate information is referenced to the North American Datum of 1983 (NAD 83).

Vertical coordinate information is referenced to the North American Vertical Datum of 1988 (NAVD 88).

Elevation, as used in this report, refers to distance above the vertical datum.

Stage, as used in this report, refers to the distance above the datum of the U.S. Geological Survey streamgage 05536890, Chicago Sanitary and Ship Canal near Lemont, Illinois, which is 551.76 feet above NAVD 88.

Supplemental Information

A water year is the 12-month period from October 1 through September 30 and is designated by the calendar year in which it ends (water year 2019 is the period beginning October 1, 2018, and ending September 30, 2019).

Abbreviations

ADCP	acoustic Doppler current profiler
ADVM	acoustic Doppler velocity meter
AVM	acoustic velocity meter
CAWS	Chicago Area Waterway System
CV	coefficient of variation
DRE	data reduction equation
EIV	errors in variables
FOSM	first-order second moment
GLS	generalized least squares
IVR	index-velocity rating
LMDA	Lake Michigan Diversion Accounting
OLS	ordinary least squares
Qm	discharge measurement
R^2	coefficient of determination
RMSE	root-mean square error
SE	standard error
TRC	technical review committee
USACE	U.S. Army Corps of Engineers
USGS	U.S. Geological Survey
WLS	weighted least squares
WY	water year
X^2	chi squared

Uncertainty Analysis of Index-Velocity Meters and Discharge Computations at the Chicago Sanitary and Ship Canal near Lemont, Illinois, Water Years 2006–16

By Thomas M. Over,[1] Marian Muste,[2] James J. Duncker,[1] Heng-Wei Tsai,[2,3] P. Ryan Jackson,[1] Kevin K. Johnson,[1] Frank L. Engel,[1] and Crystal D. Prater[1]

Abstract

Monitoring discharge in the Chicago Sanitary and Ship Canal is critical for the accounting done by the U.S. Army Corps of Engineers of the diversion of water from Lake Michigan to the Mississippi River Basin by the State of Illinois. The primary streamgage used for this discharge monitoring, the Chicago Sanitary and Ship Canal near Lemont, Illinois (U.S. Geological Survey station 05536890), is operated by the U.S. Geological Survey as an index-velocity station and at the time of this study (water years 2006–16) had two continuous velocity meters (an acoustic Doppler velocity meter and an acoustic velocity meter) and a water-level sensor, among other instruments. Discharge is computed at the streamgage using an index-velocity rating developed by linear regression of the velocity meter values fitted to discharges intermittently measured with an acoustic Doppler current profiler. In this study, the uncertainties of the velocity meters and stage sensors were estimated using a type B (judgment-based) approach, and measured discharge uncertainties were taken from those provided by a common acoustic Doppler current profiler data processing software tool, QRev. The velocity meter uncertainties, expressed as standard deviations, were estimated to be about 2.5 percent of velocity except near zero, where they exceeded that fraction, whereas for the acoustic Doppler current profiler uncertainties, when converted to mean channel velocity, 2.5 percent of velocity was determined to be a lower bound. The estimated velocity meter and measured discharge uncertainties were compared to index-velocity ratings developed from regression analyses of two types: (1) those that allow specification of measurement uncertainties and (2) ordinary least squares (OLS) regression, which does not. Based on the linearity of the index-velocity rating and the approximate agreement of the distributions of the fitting and prediction velocities, the assumptions required for unbiased prediction by OLS regression were determined to be approximately satisfied. From the regression residuals, it was determined that the estimated measurement uncertainties are too small, too similar between acoustic velocity meter and acoustic Doppler velocity meter velocities, and possibly too strongly dependent on velocity. Large, non-Gaussian OLS regression residuals also were observed. The uncertainty of annual mean discharge computed using the different regressions also was considered and was determined to be strongly dependent on the assumed measurement uncertainty. Because the assumptions required for OLS regression to give unbiased and variance-maintaining predictions were determined to be approximately satisfied, the results of discharge computation using the index-velocity rating based on OLS regression were deemed to be reliable. These results indicate about 0.8-percent uncertainty in the computed discharge as measured by the coefficient of variation at the annual time scale when using the acoustic Doppler velocity meter and 1.2-percent uncertainty with the acoustic velocity meter. It may be possible to improve the accuracy of the computed discharge and its uncertainty by further examining the measurement uncertainties and addressing differences in the distributions of the velocities used in fitting the index-velocity ratings and those used in prediction. Although the index-velocity ratings and computed discharges presented in this study are similar to those used in computing the published discharge at the study streamgage, the values presented in this report are not intended to replace the published discharge.

Introduction

From 1836 to 1922, a series of canals was built to connect Lake Michigan (fig. 1) to the Illinois River (fig. 1; appendix 2, slides 2–3). In 1900, construction of the Chicago Sanitary and Ship Canal was completed, effectively "reversing" the flow of the Chicago River and protecting the city's drinking water supply in Lake Michigan. The canal breached a low drainage divide between the Lake Michigan Basin and the Mississippi River Basin (fig. 1; appendix 2, slide 3), and

[1]U.S. Geological Survey.

[2]University of Iowa.

[3]U.S. Army Corps of Engineers.

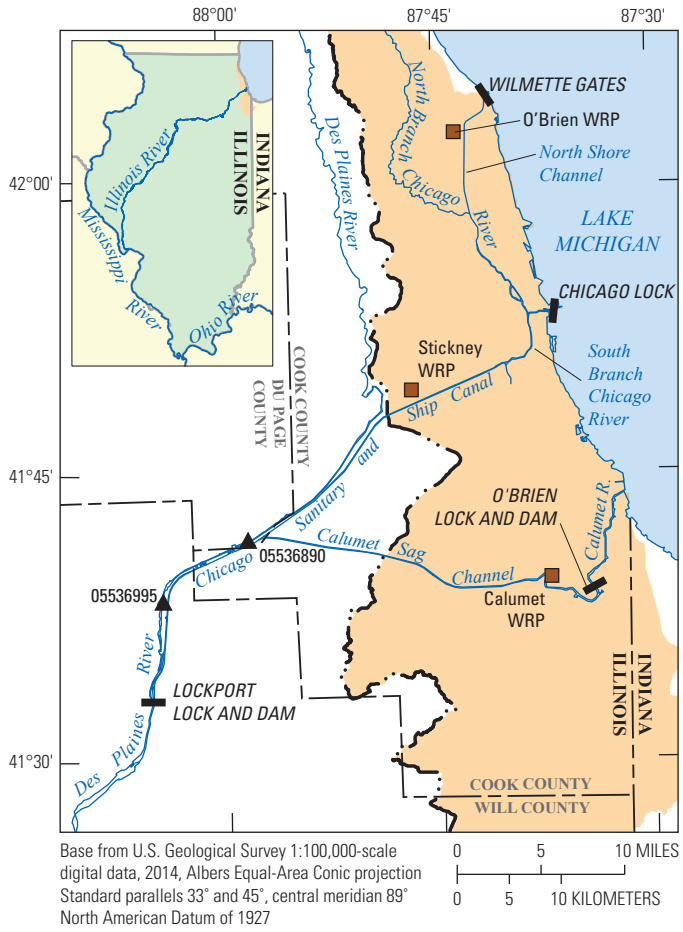

Figure 1. Locations of U.S. Geological Survey streamgages, the Chicago Sanitary and Ship Canal, the diverted Lake Michigan watershed, and related features of the Chicago Area Waterway System.

the river's flow and the sanitary sewage that the river also carried were diverted away from Lake Michigan into the Mississippi River Basin. By 1922, two additional canals had been cut across the divide, the Calumet Sag and the North Shore Channels (fig. 1; appendix 2, slide 3). Today (2021), the drinking water from Lake Michigan that is diverted down the Chicago Sanitary and Ship Canal serves a population of about 6.6 million people in the Illinois part of metropolitan Chicago (Illinois Environmental Protection Agency, 2021) and others in northwest Indiana, and the Chicago Area Waterway System (CAWS; fig. 1; appendix 2, slide 3) consists of more than 90 miles of natural and human-made channels (Duncker and Johnson, 2015). Three primary water reclamation plants serve the Chicago metropolitan area and return treated effluent to the CAWS (fig. 1; appendix 2, slide 3).

After multiple U.S. Supreme Court decrees related to the diversion of water from the Great Lakes to the Mississippi River Basin resulting from the CAWS, most recently in 1980 (Wisconsin v. Illinois, 449 U.S. 48 [1980]), the 1986 Water Resources Development Act (42 U.S.C. 1962d–20) gave the U.S. Army Corps of Engineers (USACE) the responsibility to monitor and compute the diversion. Diversion by the State of Illinois from the Great Lakes Basin is limited by the U.S. Supreme Court decree to a long-term mean of 3,200 cubic feet per second (ft^3/s; Wisconsin v. Illinois, 388 U.S. 426 [1967]; Wisconsin v. Illinois, 449 U.S. 48 [1980]). The Lake Michigan Diversion Accounting (LMDA) system was developed by the USACE-Chicago District in response to the 1986 Water Resources Development Act directive.

Under the auspices of the LMDA project and under contract to the USACE, the U.S. Geological Survey (USGS) has operated a streamgage on the Chicago Sanitary and Ship Canal since 1984 (appendix 2, slide 4). This streamgage is the primary measurement point for more than 90 percent of the diverted water. Originally, this streamgage was Chicago Sanitary and Ship Canal at Romeoville, Illinois (USGS station 05536995, hereinafter, the "Romeoville streamgage"). However, in 2005, the primary monitoring location was moved about 6 miles upstream to Chicago Sanitary and Ship Canal near Lemont, Ill. (USGS station 05536890; hereinafter, the "Lemont streamgage"), and remains there now (2021; Johnson and others, 2012).

Because of the hydraulic conditions at the Lemont streamgage, it is operated as an index-velocity station, at which at least two continuously operating meters, at least one for velocity and another for stage (water level), are used. Data from the velocity meter are converted to mean channel velocity by fitting a curve called an index-velocity rating (IVR) between its measurements and those from periodic discharge measurements. Stage data are converted to cross-sectional area with a stage-area rating, which is developed from channel geometry. The product of the rated velocity and the rated area gives the computed discharge. Except for the first two years and the last year of the period considered in this study (water years [WYs] 2006–16), the Lemont streamgage had two velocity meters, an acoustic velocity meter (AVM) and an acoustic Doppler velocity meter (ADVM), each with its own IVR. The presence of the two meters during WYs 2008–15 allows for comparisons of their results that support a more thorough evaluation than otherwise would be possible.

Uncertainties of measurements and computed discharge used in Lake Michigan diversion computations were previously analyzed by Over and others (2004) and Duncker and others (2006), who considered the velocity meters and the computed discharge in use from WYs 1997–99 at the Romeoville streamgage (the predecessor to the Lemont

streamgage as the primary discharge monitoring point for Lake Michigan diversion computations) and at one to three other streamgages. At the Romeoville streamgage, Duncker and others (2006) estimated the AVM velocity uncertainty, expressed as a standard deviation, to be about 0.0030 foot per second (ft/s) and the standard deviation of the computed discharge uncertainty at annual time scale to range from 0.6 to 2.2 percent of discharge, depending on the assumed bias of the periodic discharge measurements used in developing the IVR, with 0.6 percent corresponding to no bias and 2.2 percent to the largest bias considered.

The 1980 Supreme Court decree also stipulates that the USACE will convene the three-member technical review committee (TRC) at least once every 5 years to review and report on the methods of flow measurement and procedures for diversion accounting. The first such technical review report was published in 1981 (Espey and others, 1981), and the most recent, the eighth, was published in 2019 (Espey and others, 2019). Among the recommendations of the sixth and seventh TRC reports (Espey and others, 2009, 2014) are assessments of the uncertainties of the AVM, ADVM, and acoustic Doppler current profiler (ADCP) measurements of discharge and the computation of the resulting uncertainty of the annual total discharge.

Purpose and Scope

The purpose of this report is to respond to the recommendations of the sixth and seventh TRC reports regarding uncertainty assessments for the velocity meters, discharge measurements, and computed annual total discharge at the Lemont streamgage. This report builds on prior velocity meter and discharge uncertainty analyses by the USGS for the LMDA project (Over and others, 2004; Duncker and others, 2006), which focused on a statistical approach, using properties of the index-velocity rating regression; this report continues that approach but also investigates incorporation of measurement uncertainty in stage, index velocity, and discharge. The analyses presented in this report consist of the following:

1. a "type B" (that is, one developed using scientific judgment based on all available information regarding the sources of uncertainty) uncertainty analysis of the ADVM, AVM, and stage measurements based on "Evaluation of Measurement Data—Guide to the Expression of Uncertainty in Measurement" (Joint Committee for Guides in Metrology, 2008) at the Lemont streamgage;

2. the estimation of the uncertainties of the ADCP discharge measurements (Qms) used for calibration (that is, fitting) of the IVRs;

3. the development and analysis of two sets of IVR curves (one set each for the AVM and the ADVM) based on a newly processed dataset of corresponding ADCP and index-velocity (ADVM and AVM) measurements at the Lemont streamgage (Prater and others, 2021) and the estimated ADVM and AVM measurement uncertainties; and

4. the estimation of computed discharge and its uncertainty for selected IVR curves.

The different IVRs estimated in analysis step 3 are computed based on how the uncertainty estimates from steps 1 and 2 are used in the IVR regressions. For example, ordinary least squares (OLS) regression ignores such information, whereas weighted least squares (WLS) regression considers the uncertainties of the predictand (the y-axis variable; here, the velocity associated with the ADCP discharge). Additional types of regression considered here allow for consideration of uncertainties in the predictor (the x-axis variable; here, the index velocity) and for correlations among the uncertainties. The different IVRs arising from these additional types of regression can each be used for prediction; that is, to compute discharge using the continuous velocity data provided by the index-velocity meters and continuous cross-sectional area values computed from the continuous water-level data.

The results presented in this report are based on preliminary results presented by Over and others (2017). An updated version of the PowerPoint used in that presentation is attached to this report as appendix 2, with descriptions of the slides in appendix 1. Callouts to the slides by number have been inserted in the report text.

The Chicago Sanitary and Ship Canal near Lemont, Illinois, Streamgage

At the Lemont streamgage, the Chicago Sanitary and Ship Canal is an excavated rectangular channel about 162 feet (ft) wide, and the typical stage of 25 ft is 25–27 ft above a variable bottom elevation of 549–551.5 ft (above the North American Vertical Datum of 1988; Jackson and others, 2012; figs. 2*A*, *B*, and 3; appendix 2, slides 5 and 6). Just downstream (to the southwest) from the gage house is a sloughed bank, which reduces the cross-sectional area in that reach. A noncontact pressure transducer is used in conjunction with a gas-purge bubbler system to provide continuous stage (water-level) measurements (appendix 2, slide 7).

Two continuous velocity meters were present at the Lemont streamgage during this study: an ADVM and an AVM. The AVM was originally (2004) the primary velocity meter and the ADVM was the secondary or backup velocity meter; the order of priority was switched at the beginning of WY 2016. The AVM failed in April 2016 and has since been removed.

The ADVM is a 600-kilohertz Teledyne RD Instruments Channel Master, which has two beams that point 20 degrees upstream and downstream from the cross channel perpendicular, respectively. The ADVM is mounted on the northwest side of the channel next to the gage house, 13.2 ft above the gage datum, and during this study, it was set to return velocities

Figure 2. Views of the Chicago Sanitary and Ship Canal near Lemont, Illinois, streamgage (U.S. Geological Survey station 05536890) showing (*A*) gage house and instrumentation (modified from Jackson, 2018; photograph by Clayton Bosch, U.S. Geological Survey) and (*B*) the Chicago Sanitary and Ship Canal, looking downstream toward the streamgage during the installation of the uplooking acoustic Doppler current profiler (photograph by James Duncker, U.S. Geological Survey).

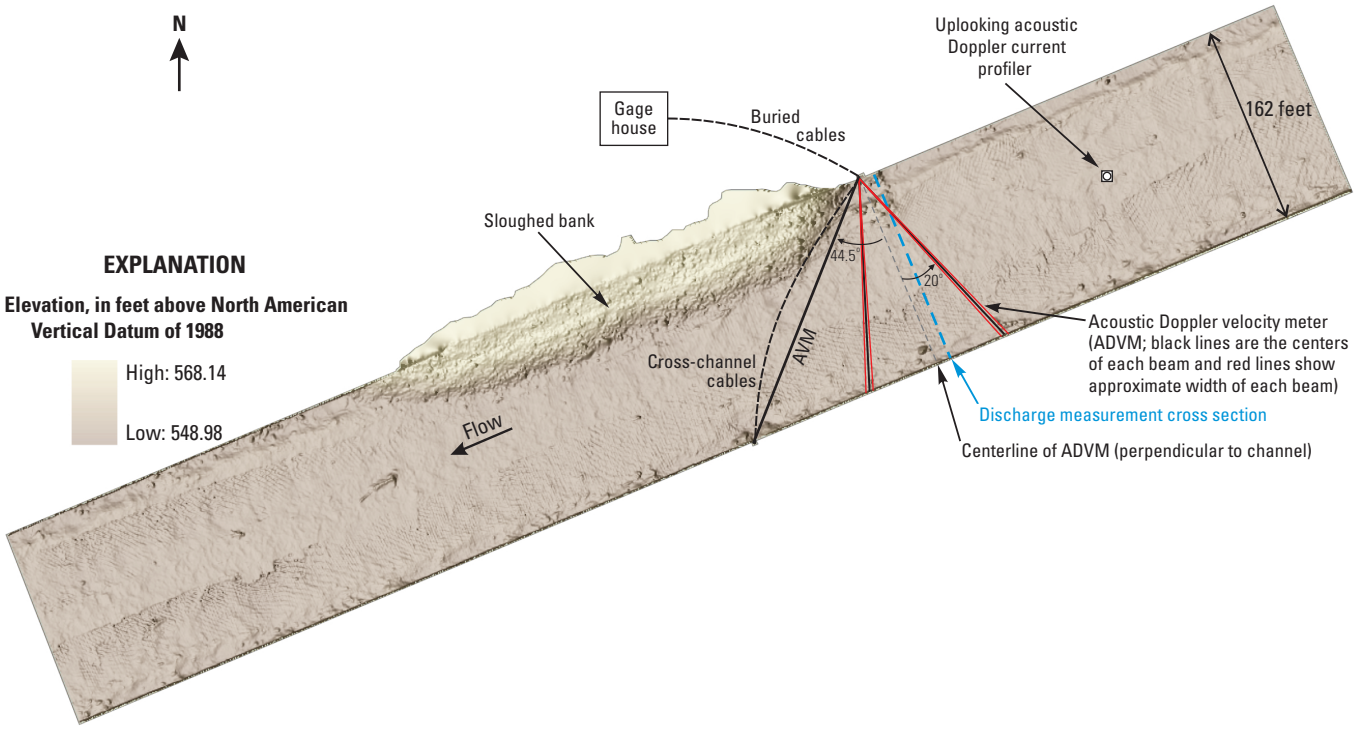

Figure 3. Instrument configurations superimposed on the channel bathymetry at the Chicago Sanitary and Ship Canal near Lemont, Illinois, streamgage (U.S. Geological Survey station 05536890). [Modified from Jackson and others, 2012; AVM, acoustic velocity meter]

in nine horizontal segments (cells) at 5 meters per cell, thus measuring the central 45 meters of the nominal 162-ft channel width. The ADVM velocity was computed from the mean of the values in the cells reporting valid data at a 1-minute time step (Jackson and others, 2012; fig. 4*A* and *B*; appendix 2, slide 8).

The AVM was an Accusonic O.R.E. 7510 with three paths, one each at 7.8, 13.2, and 18.4 ft above the gage datum, so its second path was at the same depth as the ADVM. Its transducers were placed so that the acoustic path between them had a length of 234.8 ft and was at a 44.5-degree angle relative to a perpendicular cross section. From each of the three AVM paths, 10-minute means of the velocities were averaged to obtain a composite AVM velocity for the cross section. When velocity data for all three paths were valid, a simple average was computed. If velocity data for one or two paths were missing or invalid, path coefficients were applied to the valid data before averaging, as described by Jackson and others (2012).

At the site, Qms are made using a Teldyne RD Instruments Rio Grande ADCP, mounted on a moving boat and tethered to a cross-channel tagline. From January 2014 to January 2018, an uplooking ADCP was at the site; its data were analyzed by Jackson (2018) but are not used in this study.

Approach to Uncertainty Estimation

Four steps were used in the analysis presented in this report (appendix 2, slide 9). The first step is the estimation of measurement uncertainty at the continuous sensors in use at the Lemont streamgage, consisting of the water-level sensor and the two index-velocity meters, using the first-order second moment (FOSM) method using a type B approach: AVM, ADVM, and stage. The second step is the estimation of the uncertainties of the Qms by ADCP used for calibration and fitting of the IVRs. The third step is the computation of two sets of IVRs, one each for each of the index-velocity meters. The different IVRs are distinguished by how the uncertainty estimates from the first two steps are used in the IVR regressions. In the fourth step, the different IVRs arising from the different IVR regressions are used to compute discharge using the continuous velocity data provided by the index-velocity meters and continuous cross-sectional areas computed from the continuous water-level data.

Discharge Measurement Dataset

A dataset of 155 Qms made at the Lemont streamgage between January 12, 2005, and October 23, 2013, were processed for this study using QRev (Mueller, 2016; appendix 2, slide 10). These Qms have discharges ranging from −344 to 16,794 ft^3/s with a median of 2,605 ft^3/s, have durations ranging from 162 to 3,563 seconds with a median of 831 seconds, and consist of 1 to 18 transects with a median of 4.

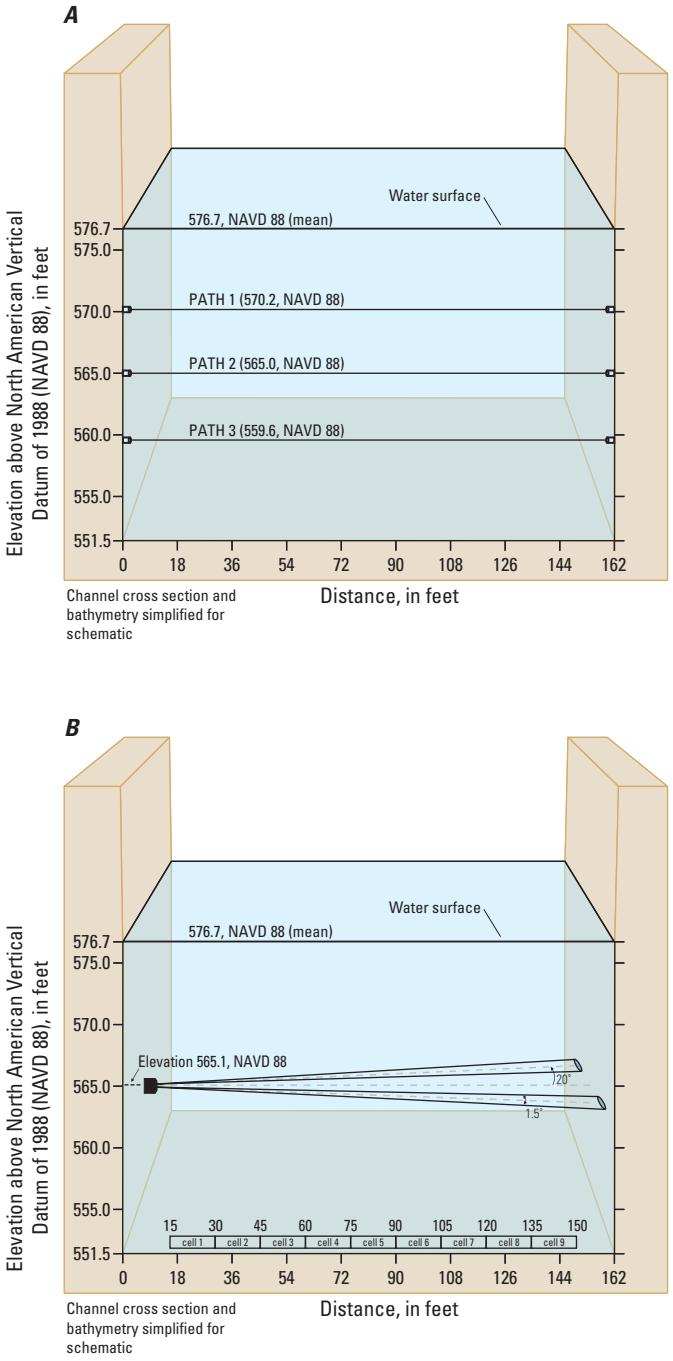

Figure 4. Channel cross section showing (*A*) the three paths of the acoustic velocity meter (looking upstream), and (*B*) acoustic Doppler velocity meter (looking upstream) deployed at the Chicago Sanitary and Ship Canal near Lemont, Illinois, streamgage (U.S. Geological Survey station 05536890). [Modified from Jackson and others, 2012]

Of these Qms, 140 have corresponding AVM velocities, 130 have corresponding ADVM velocities, and 115 have both AVM and ADVM velocities. The 115 Qms having both AVM and ADVM velocities (termed here the "common" Qms) allow comparison of IVRs developed using the two index-velocity meters with the same Qms. The dataset is available as a USGS data release (Prater and others, 2021). Select data for the aforementioned Qms also are available in the USGS National Water Information System database (U.S. Geological Survey, 2021).

Estimation of Measurement Uncertainty for Continuous Sensors

In this study, the measurement uncertainty at the continuous sensors was estimated using a "type B" analysis (that is, one developed using scientific judgment based on all available information regarding the sources of uncertainty; Joint Committee for Guides in Metrology, 2008; appendix 2, slide 11) with computations determined using the FOSM method. A type B analysis is used in this study for these sensors (AVM, ADVM, and pressure transducer) instead of a "type A" analysis, which uses statistical analysis of repeated measurements, because for applications in the field, measurement conditions cannot be controlled and, as a result, obtaining the data to complete a type A analysis is usually not possible.

The general approach to a type B analysis is as follows. First, a data reduction equation (DRE), which represents how the quantity of interest is computed as a function of directly measured quantities and their associated parameters, is developed. Then, these measured quantities and parameters are assigned uncertainties (probability distributions of their expected errors, termed "elemental uncertainties") based on scientific judgment, including information about the instruments being used and the mode of application (both the field conditions and the practices used in obtaining a measurement). The resulting fully specified DRE can then be used to propagate the errors to the quantity of interest that is described by the DRE. As a basis for scientific judgment in developing the DRE and the specifications of its parameters, the authors of this report have among them many decades of streamflow measurement experience of which a substantial fraction composes experience at the Lemont streamgage.

Error Propagation

Error propagation is commonly done in one of two ways. One is FOSM analysis, where the second moment (the variance) is approximated using first-order (Taylor series) expansion (appendix 2, slide 12). This method makes two substantial assumptions: it reduces the specified probability distributions to their variances, and it reduces the DRE to a first-order (linear) form. As such, it is exact for Gaussian errors and a linear DRE but may give erroneous results for nonlinear DREs or non-Gaussian errors (for example, errors characterized by a rectangular distribution). To check for inaccuracies resulting from the assumptions inherent in the FOSM method, the second error propagation method can be used. This method is a Monte Carlo analysis, in which simulated errors that follow the specified error distributions are directly propagated through the DRE. In this study, both methods (FOSM and Monte Carlo) were implemented using the QMSys software package developed by Qualisyst Ltd. (2015), under the assumption of Gaussian elemental uncertainties. Even for the AVM DRE, which contains substantial nonlinearity, the FOSM and Monte Carlo methods produced sufficiently similar results that only FOSM results are presented. It is important to note that the approximate agreement of the FOSM and Monte Carlo results extended to the full distributions, not just the variance; that is, the Monte Carlo error distributions were approximately Gaussian.

Uncertainty in the FOSM method is computed as the variance, that is, the second moment, of some quantity Y, which is a function of one or more variables:

$$Y=g\,(X_1, X_2, \ldots, X_n), \tag{1}$$

where

Y is the quantity being computed;
$g()$ is the function that gives Y given the values of $X_1, X_2, \ldots, X_n$: and
$X_1, X_2, \ldots, X_n$ are the variables that predict Y through the function $g()$.

Using properties of variance and a Taylor series (first-order) expansion, variance of Y is approximately

$$\sigma_Y^2 \cong \sum_{i=1}^{n}\sum_{j=1}^{n} \left.\frac{\delta g}{\delta X_i}\right|_{\mu} \left.\frac{\delta g}{\delta X_j}\right|_{\mu} \sigma_{X_i, X_j} \tag{2}$$

where

σ_Y^2 is the variance of Y,
$\left.\frac{\delta g}{\delta X_i}\right|_{\mu}$ is the partial derivative of g with respect to X_i evaluated at its mean μ, and
σ_{X_i, X_j} is the covariance between X_i and X_j.

If the X variables are independent, then

$$\sigma_Y^2 \cong \sum_{i=1}^{n}\left(\left.\frac{\delta g}{\delta X_i}\right|_{\mu}\right)^2 \sigma_{X_i}^2, \tag{3}$$

For example, for $Q=AV$, where Q is discharge, A is the cross-sectional area, and V is velocity, one gets the following:

$$\sigma_Q^2 \approx \left(\frac{\delta Q}{\delta V}\Big|_\mu\right)^2 \sigma_V^2 + \left(\frac{\delta Q}{\delta A}\Big|_\mu\right)^2 \sigma_A^2 = A^2\sigma_V^2 + V^2\sigma_A^2, \quad (4)$$

where

σ_Q^2 is the variance of discharge,

$\frac{\delta Q}{\delta V}\Big|_\mu$ is the partial derivative of discharge with respect to velocity evaluated at the mean discharge,

σ_V^2 is the variance of velocity,

$\frac{\delta Q}{\delta A}\Big|_\mu$ is the partial derivative of discharge with respect to cross-sectional area evaluated at the mean discharge, and

σ_A^2 is the variance of cross-sectional area.

Equations 1–4 have been adapted from Duncker and others (2006).

Acoustic Velocity Meter Velocity

AVMs operate by measuring the time of travel of sound waves between two transducers of known separation distance and at a known angle to the flow velocity; these waves are advected by the water, so the difference in the time of travel in the direction of water flow and that of the return can be used to estimate the flow velocity (appendix 2, slide 13; Laenen, 1985). The resulting DRE (eq. 5) expresses the "line velocity" (that is, the mean water velocity along the line between the transducers) as a function of the travel times, the flow velocity-acoustic path angle, and the path length. The DRE is nonlinear in the times of travel and angle between the acoustic waves and the flow velocity.

$$V_L = \frac{B}{2\cos(A)}\left(\frac{1}{T_{DC}} - \frac{1}{T_{CD}}\right) \quad (5)$$

where

V_L is "line velocity," velocity along the acoustic path, used as index velocity;

B is the acoustic path length;

A is the angle between acoustic path and velocity; and

T_{CD}, T_{DC} are travel times of acoustic signal between the transmitter and receiver and back.

To the basic DRE that describes the AVM line velocity returned by the instrument (appendix 2, slide 13), error sources related to the field conditions, deployment practices, and data processing were added (fig. 5; appendix 2, slide 14). The elemental uncertainties for these error sources in terms of their standard uncertainties (standard deviations), which fully characterize an assumed Gaussian distribution assuming a zero mean, were estimated (table 1; appendix 2, slide 15) and entered into the QMSys software along with the DRE, and error propagation computations were carried out. The absolute uncertainty for the error source OC_3, which refers to the time synchronization between the AVM and Qms used in rating curve development, is indicated as "not applicable" in table 1 (appendix 2, slide 15) and does not contribute to the AVM

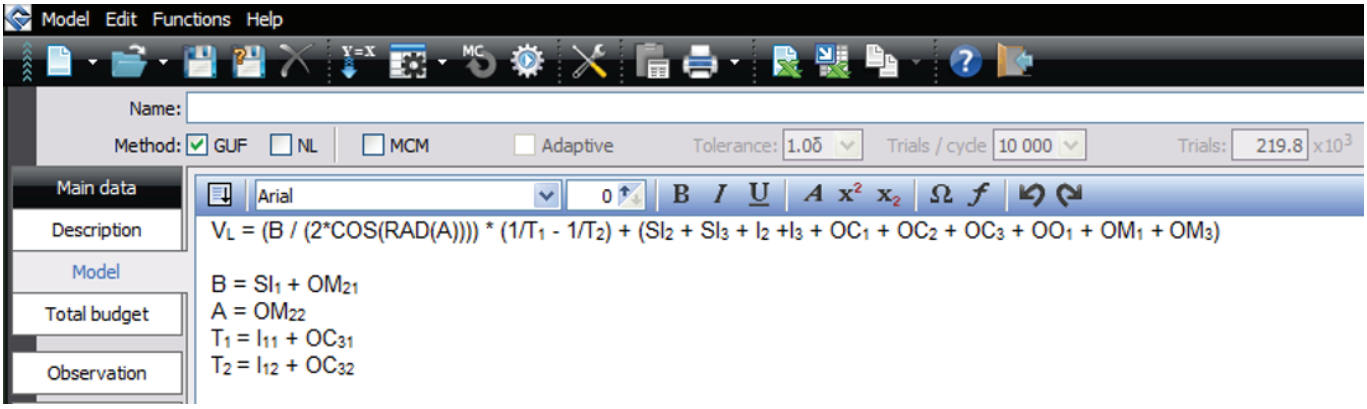

Figure 5. Part of QMSys software input window showing the expanded data reduction equation used to compute acoustic velocity meter uncertainties. [V_L, index velocity; B, acoustic path length; COS, cosine function; RAD, radian function; A, angle between acoustic path and velocity; T_1, downstream travel time; T_2, upstream travel time; SI_2, error from changes in spatial flow distribution; SI_3, error in acoustic path angle; I_2, error from instrument resolution; I_3, deprecated error set to zero; OC_1, error from sampling frequency; OC_2, error from sampling time; OC_3, error from time synchronization; OO_1, error from operational issues; OM_1, error from wind-induced shear; OM_3, error from temporary changes in flow distribution; OM_{21}, error in acoustic path length from acoustic path deflection; OM_{22}, error in angle between acoustic path and velocity from acoustic path deflection; I_{11}, error in downstream travel time; OC_{31}, error in downstream travel time from time synchronization; I_{12}, error in upstream travel time; OC_{32}, error in upstream travel time from time synchronization]

Table 1. Elemental uncertainties for acoustic velocity meter velocity at low flow.

[Low flow selected as discharge = 1,300 cubic feet per second; velocity (V) = 0.322 foot per second (ft/s); stage = 24.92 feet; %, percent; e, denotes exponentiation; nsec, nanosecond; B, acoustic path length; A, angle between acoustic path and velocity]

Name	Notation	Error category	Absolute uncertainty	Contribution to total uncertainty (ft/s)[1]
Acoustic path length	SI_1	Site and installation	0.02%	8e−7
Changes in spatial flow distribution	SI_2	Site and installation	1%	0.001258
Acoustic path angle	SI_3	Site and installation	0.17%	0.000036
Travel time	I_1	Instrument	30 nsec	0.001056
Instrument resolution	I_2	Instrument	0.001 ft/s	0.000121
Sampling frequency	OC_1	Operation—configuration	1%	0.001258
Sampling time	OC_2	Operation—configuration	0	0
Time synchronization	OC_3	Operation—configuration	Not applicable[2]	0
Operational issues	OO_1	Operation—operator	0	0
Wind-induced shear	OM_1	Operation—measurement	1%	0.001258
Acoustic path deflection	OM_2	Operation—measurement	1% of B, A	0.001992
Temporary changes in flow distribution	OM_3	Operation—measurement	1%	0.001258
Total				**0.00824 (2.56% of V)**

[1]Computed as the square root of the variance associated with this component.

[2]Not applicable to acoustic velocity meter velocity by itself but applicable when used in rating curve development.

uncertainty computation because it does not contribute to the AVM velocity uncertainty itself. The error sources with zero absolute uncertainties in table 1 (appendix 2, slide 15) were deemed to be negligible.

Based on the proposed DRE and estimated elemental errors, AVM velocity errors at a range of velocities from −1.5 to 6 ft/s were determined. For example, for "low flow" conditions in the Chicago Sanitary and Ship Canal, which are defined here as discharge of 1,300 ft^3/s, stage of 24.92 ft, velocity of 0.322 ft/s, and cross-sectional area of 4,037 square feet), the AVM error expressed as a standard deviation (the "standard uncertainty") was estimated by using the FOSM method as 0.00824 ft/s or 2.56 percent (table 1; appendix 2, slide 15) and as 0.00822 ft/s and approximately Gaussian by using the Monte Carlo method (fig. 6*B*; appendix 2, slide 16, lower left). The largest contributor was acoustic path deflection (OM_2), which contributed almost 0.002 ft/s of the error, followed by changes in spatial flow distribution (SI_2), sampling frequency (OC_1), travel time (I_1), wind-induced shear (OM_1), and temporary changes in flow distribution (OM_3), which together contributed about 0.006 ft/s, or most of the remainder (table 1; appendix 2, slide 15; fig. 6*A*; appendix 2, slide 16, upper right). Because changes in spatial flow distribution, sampling frequency, wind-induced shear, and temporary changes in flow distribution are expressed in percentages of the line velocity (each 1 percent), these phenomena scale directly with it, and thus, go to zero when the line velocity is zero and grow linearly with line velocity as it increases.

The largest contributor to uncertainty at low flow conditions, acoustic path deflection, is expressed as a fraction of the acoustic path length (B) and the angle between the acoustic path and flow velocity (A), which remain constant regardless of flow velocity, so it also remains constant.

Acoustic Doppler Velocity Meter Velocity

The basic DRE for ADVM velocity (appendix 2, slide 17) indicates the principle of operation of an ADVM (Morlock and others, 2002).

$$V_i = \frac{F_d}{2F_s} C \tag{6}$$

where

V_i is the velocity along the acoustic path,
F_d is the Doppler shift of received frequency,
F_s is the transducer transmit frequency, and
C is the speed of sound.

Some fraction of the sound waves ("pings") emitted by the instrument that strike scatterers, which are assumed to be carried along passively in the water, returns along the acoustic paths (fig. 4*B*; appendix 2, slide 8, right) to the transducer. According to the Doppler effect, the frequency of the returning echoes is shifted in proportion to the component of the velocity of the scatterers

A

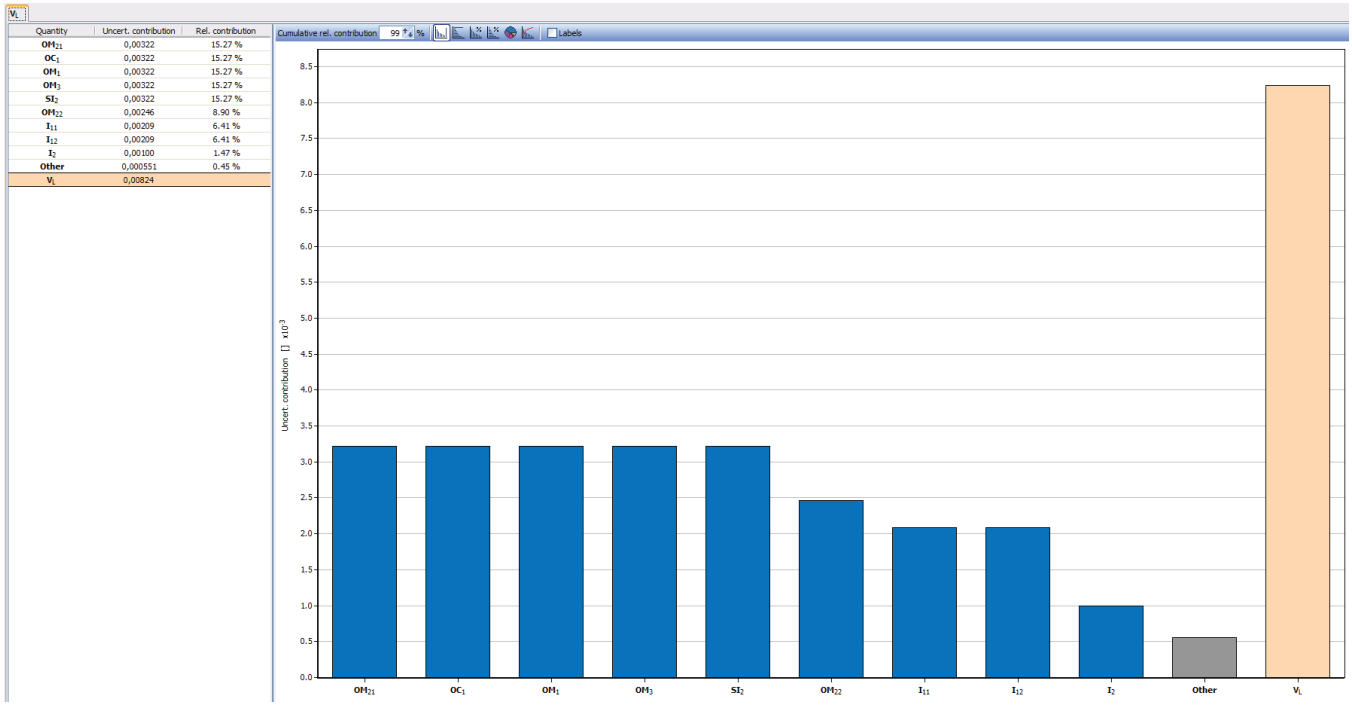

B

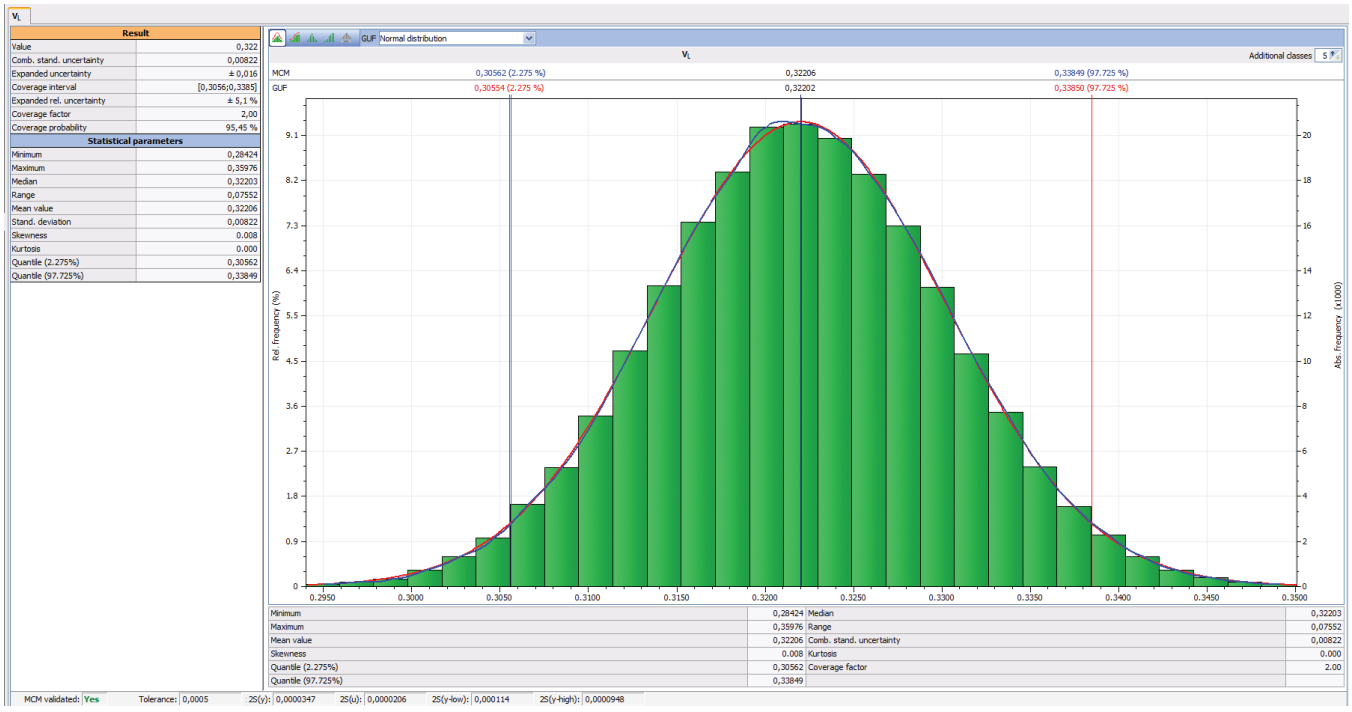

Figure 6. Acoustic velocity meter uncertainties—first-order second moment estimates from QMSys software. (*A*) Absolute and relative contributions of elemental uncertainties and (*B*) comparison of distributions of first-order second moment and Monte Carlo results.

along the acoustic path such that the ratio of the Doppler shift to the transmit frequency (F_d/F_s) is proportional to the ratio of the velocity along the acoustic path to the speed of sound (V_i/C). Because there are two beams in the horizontal plane at an angle to each other (fig. 4*B*; appendix 2, slide 8, right), the components of velocity in that plane are resolvable. For general information on site selection, installation, and configuration of ADVMs in index-velocity applications, see Levesque and Oberg (2012). As deployed at the Lemont streamgage, the resulting velocities are returned in nine 5-meter bins covering most of the distance across the channel, which are averaged to obtain a single mean velocity for each time step. The uncertainty estimation was developed in terms of the mean velocity as indicated in the expanded DRE (fig. 7; appendix 2, slide 17).

As with the AVM, ADVM velocity errors at a range of velocities from −1.5 to 6 ft/s were estimated based on the adopted DRE and estimated elemental errors (table 2; appendix 2, slide 18). The errors from sources with absolute uncertainties listed as zero in table 2 (appendix 2, slide 18) were deemed to be negligible. The elemental uncertainty for the error source OM_2 (acoustic path deflection) is indicated as "not determined" in table 2 (appendix 2, slide 18); therefore, it does not contribute to the ADVM uncertainty computation. The actual value of this uncertainty is not zero; rather, it is unknown because the experiments needed to determine its magnitude are beyond the scope of this study. In addition, the effect of errors in the temperature sensor on the ADVM (which is used to compute the speed of sound in the velocity computation) was not considered in this study.

The error sources denoted as SI_2 and OM_3 refer to changes in flow distribution (changes in spatial flow distribution and temporary changes in flow distribution, respectively). The first source of uncertainty (SI_2) refers to the effects of nonhomogeneous horizontal layers and a varying cross-sectional flow structure in the measurement volume over the range of measured velocities across seasons. The second source of uncertainty (OM_3) refers to temporary changes in flow distribution produced by barge passes or similar operations in the Chicago Sanitary and Ship Canal because of operations of the controlling structures.

At the same low flow conditions considered for the AVM (with a mean channel velocity of 0.322 ft/s) and for the estimated elemental uncertainties, the ADVM standard uncertainty was estimated as 0.0118 ft/s or 3.66 percent including consideration of salinity and 0.117 ft/s or 3.63 percent without consideration of salinity. Under these conditions, the largest contributors to the uncertainty were accuracy (I_1) and changes in spatial flow distribution (SI_2), which contributed about 0.0036 and 0.0035 ft/s, respectively, or about 60 percent of the total. Most of the remainder is estimated to come from resolution (I_2), factory settings (I_3), analytical methods (I_4), wind-induced shear (OM_1), and temporary changes in flow distribution (OM_3), which each contribute about 0.0009 ft/s and together contribute about 38 percent (table 2; appendix 2, slide 18). Of these sources, accuracy, resolution, factory settings, and analytical methods are estimated to have constant effects regardless of the flow velocity, whereas uncertainty arising from changes in spatial flow distribution, wind-induced shear, and temporary changes in flow distribution scale linearly with flow velocity and thus go to zero when the flow velocity does.

Acoustic Velocity Meter and Acoustic Doppler Velocity Meter Velocity Uncertainty Results

The results of applying FOSM analysis in a type B approach for index-velocity measurements at the Lemont streamgage indicate that AVM and ADVM standard uncertainties are generally similar and scale with flow velocity, V, approximately as $0.025V$ (fig. 8; appendix 2, slide 19). In addition, for both meters, the estimated standard uncertainties are mirrored around a flow velocity of zero. The ADVM uncertainties are somewhat higher, especially, in relative sense, near zero flow velocity, where the ADVM standard uncertainty is predicted as 0.0087 ft/s and the AVM standard uncertainty as 0.0031 ft/s. However, at a flow velocity of 6 ft/s, the ADVM and AVM standard uncertainties are predicted as 0.147 and 0.142 ft/s (2.45 and 2.37 percent), respectively. For comparison, Laenen (1985) indicated that single-path AVM systems may achieve accuracies of 3 percent and multipath systems may achieve accuracies of 1 percent. Duncker and others (2006) estimated the standard uncertainty of the AVM at the Romeoville streamgage as 0.0030 ft/s, but they did not consider operational error components. Le Coz and others (2008), testing the accuracy of a single horizontal ADVM, detected deviations from ADCP measurements within 5 percent within 60 meters of the ADVM.

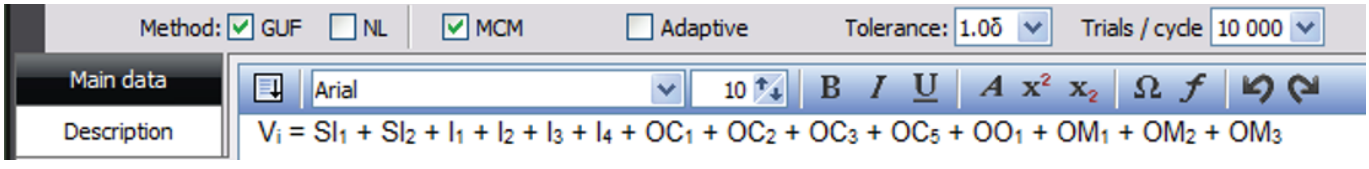

Figure 7. Expanded data reduction equation as used for uncertainty estimation of acoustic Doppler velocity meter velocities in QMSys. [V_i, velocity along acoustic path; SI_1, beam orientation error; SI_2, error from changes in spatial flow distribution; I_1, error from instrument accuracy; I_2, error from instrument resolution; I_3, error from factory settings; I_4, error from instrument analytical methods; OC_1, error from measurement volume setting; OC_2, error from sampling frequency; OC_3, error from sampling time; OC_5, compass error; OO_1, salinity input error; OM_1, error from wind-induced shear; OM_2, acoustic path deflection error; OM_3, error from temporary changes in flow distribution]

Table 2. Elemental uncertainties for acoustic Doppler velocity meter at low flow.

[Low flow selected as discharge = 1,300 cubic feet per second; velocity (V) = 0.322 foot per second (ft/s); stage = 24.92 feet; %, percent; mm/s, millimeter per second]

Name	Notation	Error category	Absolute uncertainty	Contribution to total uncertainty (ft/s)[1]
Beam orientation	SI_1	Site and installation	0	0
Changes in spatial flow distribution	SI_2	Site and installation	2%	0.003501
Accuracy	I_1	Instrument	2 mm/s	0.003634
Resolution	I_2	Instrument	1 mm/s	0.000908
Factory settings	I_3	Instrument	1 mm/s	0.000908
Analytical methods	I_4	Instrument	1 mm/s	0.000908
Measurement volume setting	OC_1	Operation—configuration	0	0
Sampling frequency, sampling time	OC_2, OC_3	Operation—configuration	0, 0	0, 0
Data logger, compass	OC_4, OC_5	Operation—configuration	0, 0	0, 0
Salinity input	OO_1	Operation—operator	0.463%	0.000187
Wind-induced shear	OM_1	Operation—measurement	1%	0.000875
Acoustic path deflection	OM_2	Operation—measurement	Not determined	0
Temporary changes in flow distribution	OM_3	Operation—measurement	1%	0.000875
Total				**0.0118 (3.66% of V)**

[1]Computed as the square root of the variance associated with this component.

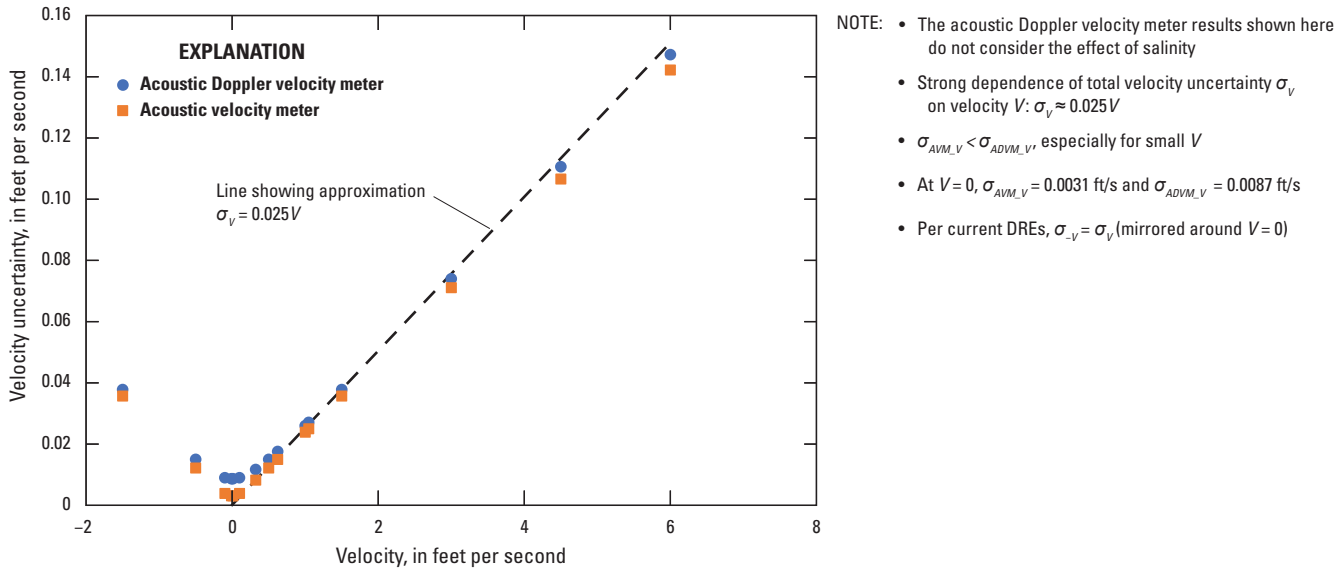

Figure 8. Comparison of predicted acoustic velocity meter and acoustic Doppler velocity meter velocity uncertainties. [σ_V, velocity uncertainty; ≈, about; σ_{AVM_V}, acoustic velocity meter velocity uncertainty; <, less than; σ_{ADVM_V}, acoustic Doppler velocity meter velocity uncertainty; ft/s, foot per second; DRE, data reduction equation; σ_{-V}, uncertainty of negative velocity]

Water Level from the Pressure Transducer

The water-level sensor deployed at the Lemont streamgage is a gas-purge bubbler system, wherein nitrogen is bubbled through the orifice line (fig. 2*A*; appendix 2, slide 5, left) and out through a fixed orifice mounted at the bottom of the canal. The water pressure at the orifice is transmitted through the orifice and measured and converted to stage by a nonsubmersible pressure transducer in the gage house. General information on water-level measurement methods and associated error sources is available in Sauer and Turnipseed (2010). A part of the QMSys software input window showing the DRE used to estimate water-level uncertainty is shown in figure 9 (appendix 2, slide 20).

The factors for which the elemental errors were used to model the water-level uncertainty in this study consist of local disturbances (SI_2), accuracy of the meter (I_1), resolution (I_2), gage offset (OC_1), and periodic stage correction (OC_4); the other factors considered were deemed to be negligible and were set to zero (table 3; appendix 2, slide 21). Of the factors used in the uncertainty modeling, local disturbances had the largest effect, contributing about 54 percent of the total estimated standard uncertainty of 0.0271 ft. Resolution, gage offset, and periodic stage correction each contributed about 13.6 percent for a total contribution of about 41 percent. Only accuracy scales with the water level, but with an absolute uncertainty of 0.02 percent of stage that varies over a fairly small range, it does not cause the water-level uncertainty to change with stage, resulting in a constant standard uncertainty of 0.0271 ft for stage from 22 to 29 ft (the range of stage observed in this study). This uncertainty may be compared to the USGS policy regarding maximum stage uncertainty of at most 0.01 ft or 0.20 percent of stage, whichever is larger (U.S. Geological Survey, 1996), which was issued in the context of the use of stage in stage-discharge ratings. At a typical stage of 25 ft, a value of 0.20 percent translates to 0.05 ft; thus, a standard uncertainty of 0.0271 ft is deemed to satisfy the policy.

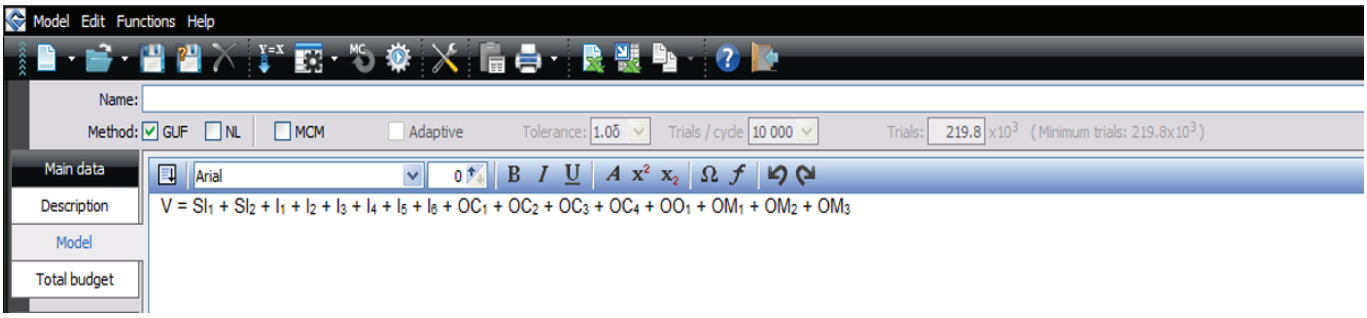

Figure 9. Water-level (stage) uncertainty estimation using the data reduction equation in QMSys. [V, velocity; SI_1, datum errors; SI_2, local disturbances; I_1, accuracy errors; I_2, resolution errors; I_3, calibration errors; I_4, data transmission errors; I_5, timing errors; I_6, data logger errors; OC_1, gage offset errors; OC_2, recorder errors; OC_3, data retrieval errors; OC_4, periodic stage correction errors; OO_1, errors from operational issues; OM_1, hydraulically induced errors; OM_2, errors from temperature effects; OM_3, errors from temporary flow disturbances]

Table 3. Elemental uncertainties for water level (stage).

[ft, foot; %, percent]

Name	Notation	Error category	Absolute uncertainty	Contribution to total uncertainty (ft)[1]
Datum errors	SI_1	Site and installation	0	0
Local disturbances	SI_2	Site and installation	0.02 ft	0.014728
Accuracy	I_1	Instrument	0.02%	0.001325
Resolution	I_2	Instrument	0.01 ft	0.003682
Calibration, data transmission	I_3, I_4	Instrument	0, 0	0, 0
Timing, data logger	I_5, I_6	Instrument	0, 0	0, 0
Gage offset	OC_1	Operation—configuration	0.01 ft	0.003682
Recorder, data retrieval	OC_2, OC_3	Operation—configuration	0, 0	0, 0
Periodic stage correction	OC_4	Operation—configuration	0.01 ft	0.003682
Operational issues	OO_1	Operation—operator	0	0
Hydraulically induced	OM_1	Operation—measurement	0	0
Temperature effects	OM_2	Operation—measurement	0	0
Temporary flow disturbances	OM_3	Operation—measurement	0	0
Total				**0.0271 ft**

[1]Computed as the square root of the variance associated with this component.

Estimation of Measurement Uncertainty of Discharge Measurements

The estimation of the uncertainty of Qms made with ADCPs has been an active research area (González-Castro and Muste, 2007; González-Castro and others, 2016; Moore and others, 2017; Huang, 2018; Naudet and others, 2019). In contrast with González-Castro and Muste (2007), who provide only a framework, the other aforementioned studies specify a method and, usually, provide software. At this time (2021), no method has become generally accepted. As a result, the semiempirical, approximate approach that is built into the ADCP data processing software package QRev (Mueller, 2016) was used in this study to estimate the ADCP measurement uncertainties.

The QRev approach to ADCP uncertainty considers (1) random uncertainty, computed from the variation among the transect discharges; (2) uncertainty arising from the filling of invalid data; (3) uncertainty arising from estimation of the discharge in the unmeasured area at the edges of the channel; (4) uncertainty arising from extrapolation to the unmeasured areas at the top and bottom of the channel; (5) uncertainty arising from the possibility of a moving bed (when the bottom track is the navigation reference, which it was here except for one measurement); and (6) systematic uncertainty, for which the standard uncertainty is set to 1.5 percent (appendix 2, slide 22). Because the QRev method computes random uncertainty from the transect discharges, it is in that respect a type A (empirical-statistical) method; the other components of the uncertainty are of a type B nature, being based on scientific judgment.

It is important to note that the QRev ADCP discharge uncertainty estimation method or any single-Qm uncertainty estimation method cannot account for correlations among ADCP errors, which might arise in ways including the same instrument being used for multiple consecutive measurements without recalibration or by the same hydrographer who might make certain operational choices that another hydrographer might not make. Such error correlation also might arise from unusual flow conditions that hold for one set of measurements but not another.

Further details on the computation of the components of ADCP discharge uncertainty with QRev and the corresponding results for all 155 Qms considered in this study (table 4; appendix 2, slide 23) indicate a wide ranges of values, when expressed as standard uncertainties in percent, for the random uncertainty, invalid data uncertainty, edge uncertainty, and extrapolation uncertainty, as well as for the total uncertainty. The dominant uncertainty component for Qms with the largest percentage uncertainties is random uncertainty. To allow comparison with the ADVM and AVM uncertainties (fig. 8, appendix 2, slide 19), these uncertainties are also presented in terms of the corresponding mean-channel velocity computed with the stage-area rating associated with the ADVM (the AVM results are similar) for the 115 common Qms (fig. 10; appendix 2, slide 24). Although the estimated ADVM and AVM standard uncertainties scale with velocity, V, as $0.025V$, that relation forms a lower limit for the QRev-estimated standard uncertainties of ADCP velocity, especially for lower velocities. The lower limit scaling with $0.025V$ arises generally from the sum of systematic, edge, and bottom-track test uncertainties. The high outliers, which are more common at lower velocities, arise because of occasionally large random uncertainties and extrapolation uncertainty estimates. Despite the presence of high outliers at low velocities, the fitted loess line (Helsel and others, 2020, section 10.3.1) indicates a general trend of increasing uncertainty with increasing velocity.

Across the common Qms, the root-mean square error (RMSE) of ADCP velocities (computed as shown in fig. 10 [appendix 2, slide 24] using the ADVM stage-area rating curve) is 0.0477 ft/s, whereas the ADVM and AVM velocities associated with the same measurements are 0.0356 and 0.0345 ft/s, respectively. Thus, according to the results of the uncertainty estimation methods presented so far, for the velocities to be used in fitting rating curves, the ADCP uncertainty is estimated as being about 36 percent larger in terms of RMSE than those from the ADVM and the AVM, which are themselves similar. However, as seen in figures 8 and 10 (appendix 2, slides 19 and 24), characterizing the predicted uncertainty by a single number should not distract from the fact that these estimates include strong positive dependence on velocity and, in the case of the ADCP estimates, substantial variability.

Table 4. Results of the QRev estimation of acoustic Doppler current profiler uncertainties.

Uncertainty source	Computation (in terms of standard uncertainties, in percent)	Uncertainty statistics for all 155 discharge measurements considered in this study, expressed as standard uncertainties, in percent		
		Minimum	Median	Maximum
Random uncertainty	Proportional to the coefficient of variation of the transect discharges	0.2	3.3	243
Invalid data uncertainty	10 percent of the percentage of discharge for invalid cells and ensembles	0	0	3.75
Edge uncertainty	15 percent of the percentage of discharge in the edges	0.45	1.75	7.9
Top/bottom extrapolation uncertainty	Based on variation among results of different extrapolation methods	0.05	0.2	9.45
Moving-bed test uncertainty	If bottom track used: 0.5 if no moving bed, 0.75 if moving bed is present, 1.5 percent if moving-bed test not performed; otherwise 0	0	1.5	1.5
Systematic uncertainty	Fixed at 1.5 percent	1.5	1.5	1.5
Total uncertainty		2.2	4.3	243

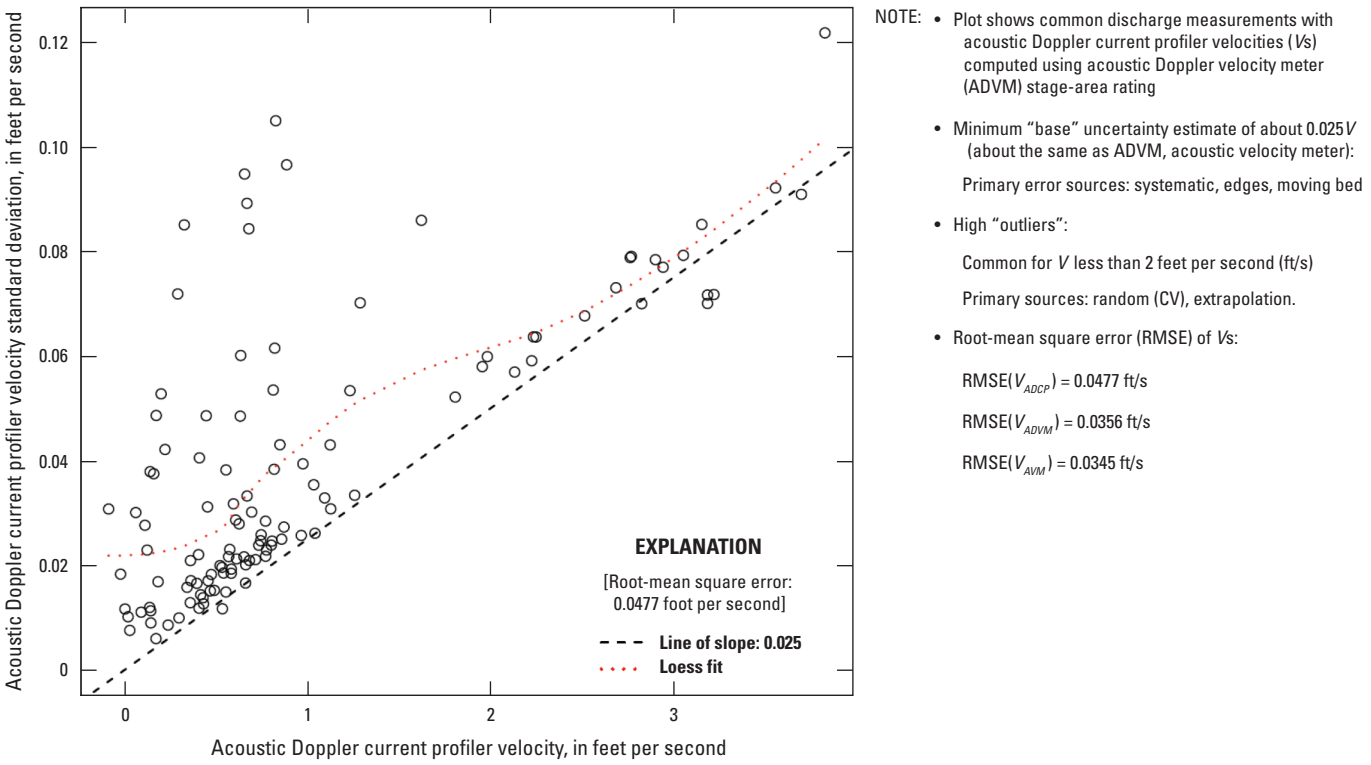

Figure 10. Estimated acoustic Doppler current profiler velocity uncertainties as a function of acoustic Doppler current profiler velocity from common discharge measurements. [CV, coefficient of variation; V_{ADCP}, acoustic Doppler current profiler velocity; V_{ADVM}, acoustic Doppler velocity meter velocity; V_{AVM}, acoustic velocity meter velocity]

Determination of Index-Velocity Ratings

In this section, the use of different types of linear regression to determine IVRs at the Lemont streamgage is presented. The USGS standard method, OLS regression, is presented first, along with its assumptions; then alternative types that allow for situations where the assumptions of OLS regression are violated are presented. The results of applying the different types of regression are presented and evaluated to assess the satisfaction of their assumptions are satisfied and, to the degree possible, the accuracy of the estimated measurement errors.

Ordinary Least Squares Regression

According to standard USGS practice (Levesque and Oberg, 2012), IVRs are developed by fitting a line (or, more generally, a curve) to the measured discharges converted to velocity by dividing by the stage-area rating corresponding to the index velocity (eq. 7) as a function of the index velocity and possibly other continuously measured quantities such as stage by OLS regression (appendix 2, slide 26).

$$V_{Qm}=Qm/Area_{index}, \quad (7)$$

where

V_{Qm} is velocity from discharge measurement,
Qm is discharge measurements, and
$Area_{index}$ is the cross-sectional area from the stage-area rating associated with the index-velocity meter.

A single straight line is fitted first (eq. 8) and is retained unless the residuals indicate otherwise.

$$V_{Qm}=a+bV_{index}, \quad (8)$$

where

V_{Qm} is velocity from discharge measurement,
a is the intercept of the IVR,
b is the slope of the IVR, and
V_{index} is velocity from the index-velocity meter.

At the Lemont streamgage, the two index-velocity meters each have their own stage-area rating (appendix 2, slide 27); the ratings differ mainly because the AVM paths cross the part of the channel where the north bank has sloughed (fig. 3; appendix 2, slide 6). Because the Qm cross section is close to the ADVM measurement cross section (labeled as "Centerline of ADVM" on fig. 3 and appendix 2, slide 6), cross-sectional areas associated with the Qms and the ADVM velocities are similar, but as described, that condition is not required in the standard USGS practice (Levesque and Oberg, 2012).

For OLS regression to be the correct model for all purposes, several assumptions are required (table 5; appendix 2, slide 28; Helsel and others, 2020, p. 228). The two most fundamental are that the response variable (y) is indeed linearly related to the predictor variable (x) and that the data used for fitting are representative of the data of interest. The first was not formally tested in this study, but it is evident from the results that if deviations from linearity are present, they are small. Regarding the second, the distributions of the index-velocity values used for fitting the IVRs and those values used for prediction later in this report compare favorably except that the IVR fitting data are missing observations in the range of 1–3 ft/s (table 6 and fig. 11*A*, *B*; appendix 2, slide 29); further, the fitting data have somewhat narrower ranges, but the central tendencies measured by the medians are close. The next two assumptions, that the residuals are homoscedastic (that is, their variance of the residuals is constant) and that the residuals are independent of the x-axis variable, are required, along with the first two assumptions, to obtain a best (minimum variance) linear unbiased estimate of y given x, and homoscedasticity is required to get the correct variance (uncertainty estimate) of the predicted y value. However, the analysis of the index velocity and ADCP measurement uncertainties indicates that neither of these assumptions is true: the residuals depend on the x-axis variable through the uncertainty of the index velocities, and they vary among the ADCP velocities as a result of its variable measurement uncertainty. The final assumption, that the residuals are normally distributed (or Gaussian), is required for the validity of tests of statistical hypotheses related to the regressions. The distribution of the residuals and its implications for statistical testing are addressed in terms of the chi-squared (X^2) test (appendix 2, slide 32).

Alternative Types of Linear Regression

Various generalized forms of linear regression have been developed to address situations where the assumptions of OLS regression are violated. This report focuses on three such generalizations that address the homoscedasticity and x-axis variable dependence of the residuals (table 7; appendix 2, slide 30): (1) WLS, in which the residuals are weighted inversely to the variance of the y values; (2) generalized least squares (GLS) regression (also called Gauss-Markov regression), in which the properties of the residuals are described by a covariance matrix with off-diagonal terms, which allows for correlations among the residuals; and (3) errors-in-variables (EIV) regression (also called generalized distance regression), in which variable uncertainties of the variables on both axes are considered. Regression models that include correlations among the errors on both the x and y axes (called generalized Gauss-Markov regression) also were considered, but results are not presented in this report because it was deemed

Table 5. Assumptions of ordinary least squares regression and their implications (modified from Helsel and others, 2020).

[*y*, response variable; *x*, predictor variable; X, the assumption is required for that purpose; --, assumption is not required]

Assumption	Purpose			
	Predict *y* given *x*	Predict *y* and a variance for the prediction	Obtain best linear unbiased estimator of *y*	Test hypotheses, estimate confidence or prediction intervals
Model form is correct: *y* is linearly related to *x*.	X	X	X	X
Data used to fit the model are representative of data of interest.	X	X	X	X
Variance of the residuals is constant (homoscedastic). It does not depend on *x* or on anything else such as time.	--	X	X	X
The residuals are independent of *x*.	--	--	X	X
The residuals are normally distributed.	--	--	--	X

unnecessarily complex for this application. For the alternative regressions, the errors were specified as predicted using the FOSM method, as described earlier. The computations were done using the R function lm (R Core Team, 2019) for OLS regression and using a translation into R of software developed by the National Physical Laboratory (2010) to implement the Technical Standard ISO/TS 28037 (International Organization for Standardization, 2010) (appendix 2, slide 31). Previously, González-Castro and Mohamed (2007), Zhang and others (2012), and Kim and others (2014) applied EIV, generalized Gauss-Markov regression, and EIV, respectively, to the problem of the fitting of stage-discharge rating curves, and they all used specified errors.

For regression models where the uncertainties are specified, the fit can be tested by applying a X^2 test (appendix 2, slide 32). This test is applied to the statistic SSR_{norm}, which is the sum of squares of the residuals normalized by their uncertainties (expressed as variances). Under the hypothesis that a linear model is correct and the errors are Gaussian with the specified variances, SSR_{norm} will be distributed as a X^2 random variable with $n-p$ degrees of freedom (Press and others, 1992, p. 653–655), where n is the number of data points used and p is the number of parameters fitted. When SSR_{norm} is too large, then at least one of the assumptions (linearity or Gaussianity with specified variances) is wrong.

Because there are known to be errors in the x-axis variable, the true model (that is, the true relation between the index velocity measured without error and the true cross-sectional velocity) has a steeper slope and smaller intercept than that obtained by OLS regression. However, because the magnitudes of the errors in the x-axis variable are unknown, it is not known whether the alternative regressions presented in this report (tables 8–11; appendix 2, slides 37–40) are closer to the true model than is the OLS regression. The question of whether or not the true model needs to be estimated is a subtle one. Sometimes an estimate of the true effect of some predictor is desired for its own sake. In the present context, that of prediction, it is often the case, as is done here, that the prediction is done using uncertain measurements from the same population as was used for the regression fit, in which case, the true model is needed only if the fitting data and the prediction data are distributed differently (Fuller, 1987, section 1.6.3; Buonaccorsi, 2010, section 4.8). Here, as described previously and as listed in table 6 and shown in figure 11*A*, *B* (appendix 2, slide 29), the fitting and prediction data are broadly similar in distribution, although proportionally fewer high-velocity measurements are in the fitting data than in the prediction data. The other case where the true model may be needed for prediction is to determine the effect of changes in the predictor as opposed to its measured value, which is relevant if the predictor can be controlled.

Table 6. Empirical distributions of acoustic Doppler velocity meter and acoustic velocity meter velocity data.

[%, percent; ADVM, acoustic Doppler velocity meter; IVR, index-velocity rating; ft/s, foot per second; AVM, acoustic velocity meter]

Data type	Number of data points	Mean	Minimum	1% quantile	10% quantile	Median	90% quantile	99% quantile	Maximum
ADVM velocities used for IVRs, ft/s	130	0.978	−0.036	0.034	0.183	0.68	2.78	3.69	3.88
ADVM prediction velocities, ft/s	464,077	0.685	−0.28	0.061	0.269	0.57	1.19	3.00	4.58
AVM velocities used for IVRs, ft/s	140	0.947	−0.037	−0.003	0.195	0.62	2.74	3.60	4.03
AVM prediction velocities, ft/s	509,996	0.719	−0.390	0.030	0.280	0.61	1.23	3.11	4.80

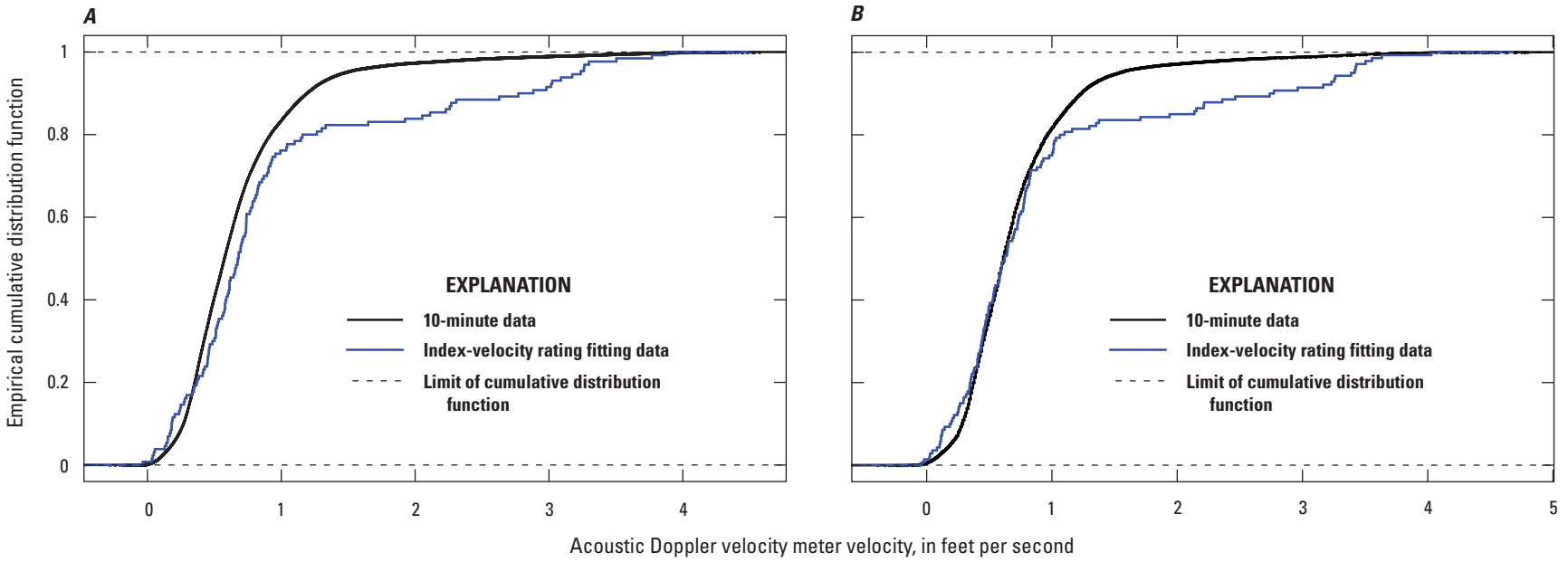

Figure 11. Empirical distributions of (*A*) acoustic Doppler velocity meter and (*B*) acoustic velocity meter velocity data.

Table 7. Regression methods considered.

[ADCP, acoustic Doppler current profiler]

Regression method	Are errors specified?	Are errors on the x (index velocity) axis considered?	Is correlation of ADCP errors considered?	Software packages used
Ordinary least squares (OLS)	No	No	No	R (lm function)
Weighted least squares (WLS)	No	No	No	R (lm function)
Weighted least squares (WLS)	Yes	No	No	R (lm) and [1]TS28037
Gauss-Markov regression (also called generalized least squares: GLS)	Yes	No	Yes[2]	TS28037
Generalized distance regression (also called errors-in-variables regression: EIV)	Yes	Yes	No	TS28037
Generalized Gauss-Markov regression[3]	Yes	Yes	Yes	TS28037

[1]TS28037 refers to "Software to Support ISO/TS 28037:2010(E)" (National Physical Laboratory, 2010).

[2]Two assumptions on correlations of the ADCP errors were tested: (1) that those measurements made in immediate succession have correlations of 0.5, and (2) that all the ADCP measurements are correlated with a correlation equal to 0.1.

[3]Basic results with generalized Gauss-Markov regression were computed but are not presented here to avoid unnecessary complexity.w

Table 8. Intercept, slope, and chi-squared test statistics for acoustic Doppler velocity meter-based index-velocity ratings for selected regression methods and error specifications.

[IV, index velocity; ADCP, acoustic Doppler current profiler; ft/s, foot per second; SE, standard error; SSR_{norm}, sum of squares of the residuals normalized by their uncertainties; *Prob*, probability; X^2_{n-p}, chi-squared random variable with $n-p$ degrees of freedom, where n is number of data points used and p is the number of parameters fitted; >, greater than; OLS, ordinary least squares; N/A, not applicable; WLS, weighted least squares; <, less than; e, denotes exponentiation; GMR, Gauss-Markov regression; GLS, generalized least squares; GDR, generalized distance regression; EIV, errors in variables]

Regression method	Are errors specified?	Are IV errors considered?	Correlation of ADCP errors	Intercept (ft/s)	Slope	Intercept SE (ft/s)	Slope SE	Correlation (intercept, slope)	SSR_{norm}	$Prob(X^2_{n-p}>SSR_{norm})$ ($n-p$=128)
OLS	No	No	None	−0.0071	0.9740	0.0073	0.0054	−0.727	N/A	N/A
WLS	Yes	No	None	−0.0336	1.0017	0.0028	0.0049	−0.747	743.3	<1e−16
WLS	[1]Yes × 2	No	None	−0.0336	1.0017	0.0056	0.0097	−0.747	185.5	0.00068
GMR (GLS)	Yes	No	[2]sel.corr.=0.5	−0.0383	1.0066	0.0032	0.0062	−0.753	932.6	<1e−16
GMR (GLS)	[1]Yes × 2	No	[2]sel.corr.=0.5	−0.0383	1.0066	0.0064	0.0125	−0.753	233.2	3.9e−8
GMR (GLS)	Yes	No	[3]corr.=0.1	−0.0359	0.9937	0.0029	0.0061	−0.246	822.0	<1e−16
GMR (GLS)	[1]Yes × 2	No	[3]corr.=0.1	−0.0359	0.9937	0.0058	0.0123	−0.246	205.5	1.6e−5
GDR (EIV)	Yes	Yes	None	−0.0349	1.0094	0.00395	0.00668	−0.754	366.6	<1e−16
GDR (EIV)	[1]Yes × 2	Yes	None	−0.0349	1.0094	0.00790	0.01336	−0.754	91.7	0.99

[1]"× 2" indicates that the estimated standard errors, both ACDP and IV, were multiplied by 2.

[2]As denoted by "sel.corr.=0.5," errors of ADCP (y-axis) measurements in immediate succession were assigned correlations of 0.5.

[3]As denoted by "corr.=0.1," errors of all ADCP (y-axis) measurements were assigned correlations of 0.1.

Table 9. Intercept, slope, and chi-squared test statistics for acoustic velocity meter-based index-velocity ratings for selected regression methods and error specifications.

[IV, index velocity; ADCP, acoustic Doppler current profiler; ft/s, foot per second; SE, standard error; SSR_{norm}, sum of squares of the residuals normalized by their uncertainties; *Prob*, probability; X^2_{n-p}, chi-squared random variable with $n-p$ degrees of freedom, where n is the number of data points used and p is the number of parameters fitted; >, greater than; OLS, ordinary least squares; N/A, not applicable; WLS, weighted least squares; <, less than; e, denotes exponentiation; GMR, Gauss-Markov regression; GLS, generalized least squares; GDR, generalized distance regression; EIV, errors in variables]

Regression method	Are errors specified?	Are IV errors considered?	Correlation of ADCP errors	Intercept (ft/s)	Slope	Intercept SE (ft/s)	Slope SE	Correlation (intercept, slope)	SSR_{norm}	$Prob(X^2_{n-p}>SSR_{norm})$ ($n-p$=138)
OLS	No	No	None	0.0400	0.9768	0.0123	0.0092	−0.707	N/A	N/A
WLS	Yes	No	None	0.0106	0.9899	0.0027	0.0048	−0.733	1,594	<1e−16
WLS	[1]Yes × 3	No	None	0.0106	0.9899	0.0081	0.0143	−0.733	177.2	0.014
GMR (GLS)	Yes	No	[2]sel.corr.=0.5	0.0014	0.9977	0.0031	0.0063	−0.746	1,748	<1e−16
GMR (GLS)	[1]Yes × 3	No	[2]sel.corr.=0.5	0.0014	0.9977	0.0093	0.0188	−0.746	194.2	0.0012
GMR (GLS)	Yes	No	[3]corr.=0.1	0.00076	0.9616	0.0029	0.0060	−0.175	1,721	<1e−16
GMR (GLS)	[1]Yes × 3	No	[3]corr.=0.1	0.00076	0.9616	0.0088	0.0181	−0.175	191.2	0.0019
GDR (EIV)	Yes	Yes	None	0.0069	1.0057	0.0032	0.0061	−0.723	1,168	<1e−16
GDR (EIV)	[1]Yes × 3	Yes	None	0.0069	1.0057	0.0095	0.0182	−0.723	129.8	0.68

[1]"× 3" indicates that the estimated standard errors, both ACDP and IV, were multiplied by 3.

[2]As denoted by "sel.corr.=0.5," errors of ADCP (y-axis) measurements in immediate succession were assigned correlations of 0.5.

[3]As denoted by "corr.=0.1," errors of all ADCP (y-axis) measurements were assigned correlations of 0.1.

Table 10. Prediction statistics for acoustic Doppler velocity meter-based index-velocity ratings for selected regression methods and error specifications.

[IV, index velocity; ADCP, acoustic Doppler current profiler; ft/s, foot per second; SE, standard error; OLS, ordinary least squares; WLS, weighted least squares; GMR, Gauss-Markov regression; GLS, generalized least squares; GDR, generalized distance regression; EIV, errors in variables]

Regression method	Are errors specified?	Are IV errors considered?	Correlation of ADCP errors	Mean bias (predicted – observed) (ft/s)	Mean SE of prediction (ft/s)	Variance ratio (predicted to observed)
OLS	No	No	None	0.00000	0.0572	0.996
WLS	Yes	No	None	0.00058	0.0627	1.054
WLS	[1]Yes × 2	No	None	0.00058	0.0627	1.054
GMR (GLS)	Yes	No	[2]sel.corr.=0.5	0.00071	0.0649	1.064
GMR (GLS)	[1]Yes × 2	No	[2]sel.corr.=0.5	0.00071	0.0649	1.064
GMR (GLS)	Yes	No	[3]corr. = 0.1	−0.00957	0.0608	1.037
GMR (GLS)	[1]Yes × 2	No	[3]corr. = 0.1	−0.00957	0.0608	1.037
GDR (EIV)	Yes	Yes	None	0.00680	0.0664	1.070
GDR (EIV)	[1]Yes × 2	Yes	None	0.00680	0.0664	1.070

[1]"× 2" indicates that the estimated standard errors, both ACDP and IV, were multiplied by 2.

[2]As denoted by "sel.corr.=0.5," errors of ADCP (y-axis) measurements in immediate succession were assigned correlations of 0.5.

[3]As denoted by "corr.=0.1," errors of all ADCP (y-axis) measurements were assigned correlations of 0.1.

Table 11. Prediction statistics for acoustic velocity meter-based index-velocity ratings for selected regression methods and error specifications.

[IV, index velocity; ADCP, acoustic Doppler current profiler; ft/s, foot per second; SE, standard error; OLS, ordinary least squares; WLS, weighted least squares; GMR, Gauss-Markov regression; GLS, generalized least squares; GDR, generalized distance regression; EIV, errors in variables]

Regression method	Are errors specified?	Are IV errors considered?	Correlation of ADCP errors	Mean bias (predicted – observed) (ft/s)	Mean SE of prediction (ft/s)	Variance ratio (predicted to observed)
OLS	No	No	None	0.00000	0.1032	0.988
WLS	Yes	No	None	−0.0169	0.1053	1.015
WLS	[1]Yes × 3	No	None	−0.0169	0.1053	1.015
GMR (GLS)	Yes	No	[2]sel.corr.=0.5	−0.0188	0.1068	1.031
GMR (GLS)	[1]Yes × 3	No	[2]sel.corr.=0.5	−0.0188	0.1068	1.031
GMR (GLS)	Yes	No	[3]corr. = 0.1	−0.0536	0.1173	0.957
GMR (GLS)	[1]Yes × 3	No	[3]corr. = 0.1	−0.0536	0.1173	0.957
GDR (EIV)	Yes	Yes	None	−0.0057	0.1070	1.047
GDR (EIV)	[1]Yes × 3	Yes	None	−0.0057	0.1070	1.047

[1]"× 3" indicates that the estimated standard errors, both ACDP and IV, were multiplied by 3.

[2]As denoted by "sel.corr.=0.5," errors of ADCP (y-axis) measurements in immediate succession were assigned correlations of 0.5.

[3]As denoted by "corr.=0.1," errors of all ADCP (y-axis) measurements were assigned correlations of 0.1.

Results of Using Ordinary Least Squares Regression

As a first step in the exploration of the IVRs for the ADVM and AVM at the Lemont streamgage, IVRs were computed using OLS regression using the 115 measurements common to both index-velocity meters. These fits (fig. 12*A*, *B*; appendix 2, slide 33) look quite good overall, having intercepts near zero and slopes near one, and they provide no reason to doubt the linearity of the ADCP velocity–index-velocity relations nor to indicate another variable is needed to explain the data; however, they raise at least two issues regarding the residuals. One is that although the type B analysis indicated that the ADVM uncertainties are somewhat larger than those from the AVM, regressions with the same set of ADCP measurements indicate that the standard errors (SEs; that is, the standard deviation of the residuals) of the AVM residuals are about twice those of the ADVM residuals (about 0.104 ft/s compared to about 0.056 ft/s when considering all the residuals [fig. 12*A*, *B*; appendix 2, slide 33] or about 0.059 ft/s compared to about 0.033 ft/s when considering just the middle 50 percent of the values [fig. 13*A*, *B*; appendix 2, slide 34]). The second is that the residuals have non-Gaussian tails, as seen from the S-shaped fits to a theoretical Gaussian distribution for which the standard deviation is computed from the middle 50 percent of the values (fig. 13*A*, *B*; appendix 2, slide 34). Although evidence of heteroscedasticity (nonconstant variance) in the residuals is strong, according to the fitted lowess line (Helsel and others, 2020, section 10.3.2), their variance increases with velocity only modestly (fig. 14*A*, *B*; appendix 2, slide 35). Whether or not this increase is as fast as would be predicted by the combination of the predicted index-velocity and ADCP errors (figs. 8 and 10 [appendix 2, slides 19 and 24], respectively) has not been determined. The similar question of whether or not the overall magnitude of the predicted errors agrees with that of the empirical residuals is addressed by applying alternative regressions, as described later in this report. Approaches to inference regarding the structure of errors when they appear only on the y axis are given for example by Faraway (2005, sections 6.1 and 6.2) for the WLS and GLS models; apparently, the inference problem is much more complicated and subtle when there are errors in the variables on both axes.

It is, however, possible to gain some qualitative insight from the regression analysis regarding which uncertainties, those of the ADCP or those of the index-velocity meters, are larger by considering the correlation between the ADVM and the AVM residuals (fig. 15; appendix 2, slide 36). The Pearson and Spearman correlations (Helsel and others, 2020, sections 8.2 and 8.3) are positive but only of moderate magnitude, indicating that the ADCP errors are roughly of about the same magnitude as the index-velocity errors. If the residuals had been strongly correlated, that fact would have indicated that the ADCP errors, which the ADVM and AVM regressions have in common, made up most of the regression residuals, whereas if the residuals had been uncorrelated, that fact would have indicated that the index-velocity errors made up most of the residuals (assuming that the ADVM and AVM errors are independent).

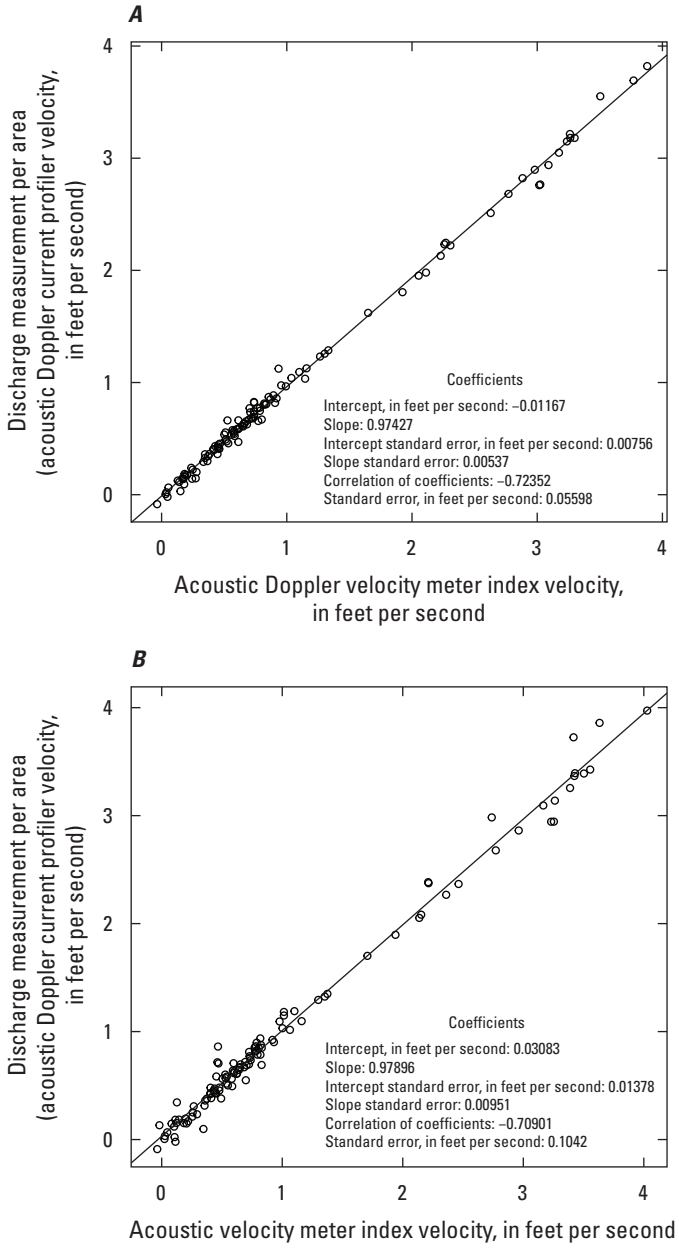

Figure 12. Comparison of ordinary least squares (*A*) acoustic Doppler velocity meter and (*B*) acoustic velocity meter index-velocity ratings (on common discharge measurements).

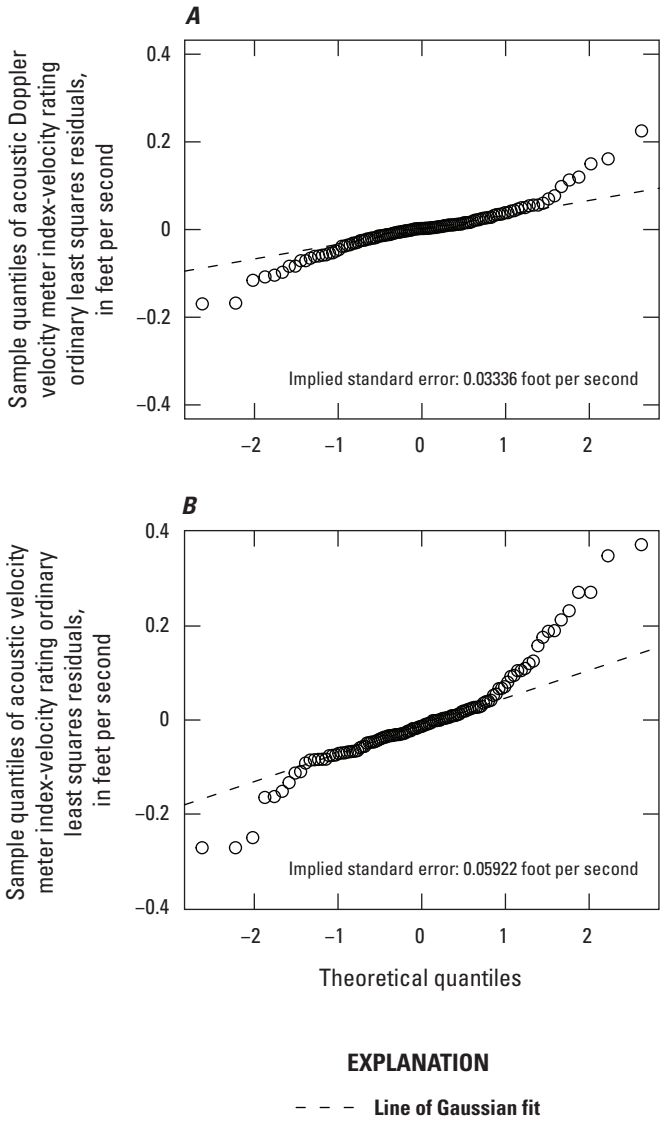

Figure 13. Distributions of ordinary least squares using Gaussian quantile-quantile plots for (*A*) acoustic Doppler velocity meter and (*B*) acoustic velocity meter index-velocity rating residuals (on common discharge measurements).

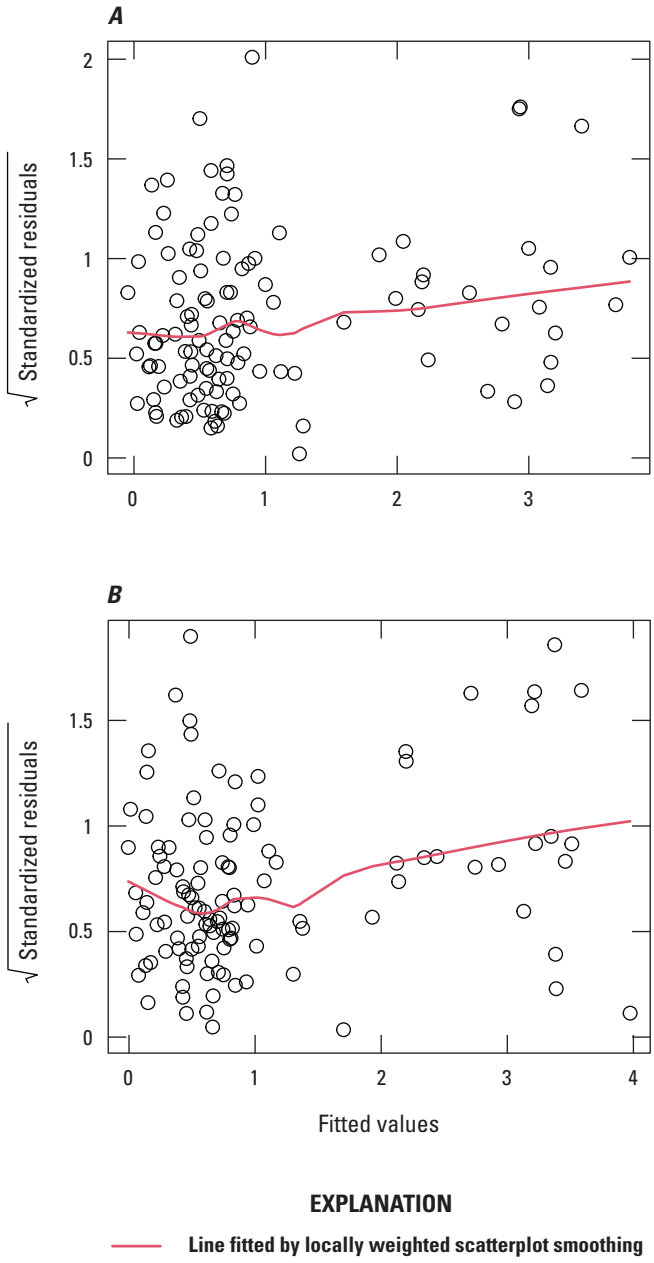

Figure 14. Heteroscedasticity of ordinary least squares using scale-location plots for (*A*) acoustic Doppler velocity meter and (*B*) acoustic velocity meter index-velocity rating residuals (on common discharge measurements).

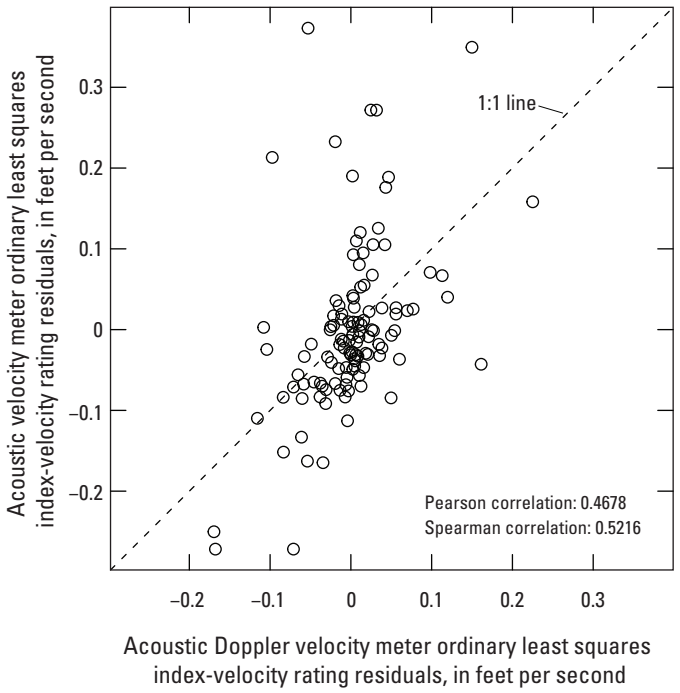

Figure 15. Index-velocity rating residuals—acoustic Doppler velocity meter versus acoustic velocity meter.

Results of Using Selected Alternative Regression Methods

The regression methods described in the "Alternative Types of Linear Regression" section were applied to the full ADVM and AVM datasets (as distinct from the common measurements used in figs. 12–15 [appendix 2, slides 33–36]). For those methods that allow for specification of errors, two sets of errors were considered: (1) the original predicted errors (figs. 8 and 10; appendix 2, slides 19 and 24) and (2) constant multiples of them (a multiple of 2 in the case of ADVM errors and 3 in the case of errors from the AVM). For the GLS method, which allows for correlations among y-axis (ADCP) errors, two assumptions were considered regarding those correlations: (1) that ADCP measurements made in immediate succession have correlations of 0.5 (indicated as "sel.corr.=0.5" in tables 8 and 9 [appendix 2, slides 37 and 38]) and (2) that all ADCP measurements are correlated at a level of 0.1 (indicated as "corr.=0.1" in tables 8 and 9 [appendix 2, slides 37 and 38]). These correlations among the ADCP errors were selected somewhat arbitrarily as a means of testing the sensitivity of the results to the presence of such correlations.

Relative to the standard method of OLS regression, all the alternative regression methods, whether they specified errors on only the y axis or both axes, except one version of GLS for the AVM data, resulted in steeper slopes and lower intercepts; thus, a counter-clockwise rotation of the regression line. That the slope of an OLS linear regression line is attenuated (biased toward zero) in the presence of errors on the x axis is well known (Fuller, 1987, chap. 1); thus, when these errors are accounted for, as indicated for the EIV regression, the line steepens and the intercept moves in the opposite direction because of its negative correlation with the slope. Based on these results and some exploratory simulations (not shown), accounting for variability in uncertainty on only the y axis using WLS regression generally has the same qualitative effect.

Other notable differences among the different regression methods include the following.

- The uncertainty (SE) of the regression coefficients also varies among the different regressions; particularly, the uncertainty increases when the specified errors increase. As described later, these uncertainties govern the uncertainty of long-term (annual) mean predictions using the corresponding IVRs.

- The p-values of the X^2 tests, $Prob(X^2_{n-p} > SSR_{norm})$, where X^2_{n-p} is a chi-squared random variable with $n-p$ degrees of freedom and SSR_{norm} is the normalized sum of squared residuals, are negligibly small for the regressions having specified errors according to the predicted errors presented previously in this report. When these errors are increased by multiplying by 2 or 3, the SSR_{norm} values decrease and the p-values become nonnegligible, but the hypothesis that the errors are Gaussian with the specified SEs remains highly unlikely, according to this test, except for the EIV regressions, which, uniquely among the methods presented, account for the effect of errors in the x-axis variable.

- The correlations of the intercepts and slope parameters have little variation among the methods, except for the GLS method with uniform y-axis uncertainty matrix correlations of 0.1, for which they are substantially reduced.

The predictions of OLS regression—for the values used to fit the regression—have a mean bias of zero and the smallest SE of prediction, but they have a reduced variance (tables 10 and 11; appendix 2, slides 39 and 40). This variance reduction in prediction with OLS regression is well known (Hirsch, 1982; Helsel and others, 2020, p. 228); its magnitude is $1-R^2$, where R^2 is the coefficient of determination of the regression. Because the R^2 values of these OLS regressions are near 1 (0.996 and 0.988 for the ADVM and AVM regressions, respectively [tables 10 and 11, respectively]), the variance reduction effect is small. Nevertheless, one effect of the steeper regression lines of all but one of the other regressions is to increase the variance of the predictions; in these results, presumably because the specified errors do not match the true errors, the variance is usually overcorrected. In addition, the predictions of the alternative regressions have a nonzero mean bias, although it is less than 0.01 ft/s in absolute value for the ADVM regressions and less than 0.02 ft/s in absolute value for the AVM regressions, other than the case of GLS regression with hypothesized correlations among all the ADCP errors.

Computation of Discharge and its Uncertainty

With an IVR, discharge is computed by multiplying the rated velocity given the observed index velocity (based on the IVR) by the rated area given the stage (based on the stage-area rating; appendix 2, slide 42).

$$Q(t)=V_{Qm}(V_{index}(t)) \times Area_{index}(h(t)), \quad (9)$$

where

$Q(t)$	is discharge at time t,
$V_{Qm}(V_{index})$	is the IVR,
$V_{index}(t)$	is continuous measurements of velocity,
$Area_{index}(h)$	is the stage-area rating, and
$h(t)$	is continuous measurements of stage.

Here, as described earlier, $V_{Qm}(V_{index})=a+bV_{index}$, where a is the intercept and b is the slope.

As described earlier, one key to the process is that the same stage-area rating (that associated with the index velocity) is used to convert measured discharge to velocity when fitting the IVR and again when reconverting the rated velocity to discharge in the discharge computation.

Given that the discharge computation is the product of two components, the rated velocity and the rated area, its uncertainty also must arise from those two components (appendix 2, slide 43). The uncertainty of the rated velocity comes from that of the IVR as embedded in the uncertainty of its parameters and its random error term. It may be that the uncertainty of the index-velocity time series used in the discharge computation needs to be considered as well, but unless this uncertainty was correlated in time over long periods (at least a month), its effects are expected to be minimal at the annual time scale (compare the results of the analysis of the effect of the uncertainty of the stage time series in computing discharge uncertainty with stage-discharge ratings by Horner and others [2018]). The uncertainty of the rated area in general depends on the uncertainty of the stage-area rating and on the uncertainty of the stage data used to compute area at each time step. The stage-area rating uncertainty has not been analyzed here because we assumed, following the argument by Duncker and others (2006, p. 28), that when the same stage-area rating is used to convert the measured discharges to velocities for use in fitting the IVR and then back to discharge when discharge is computed, its uncertainty drops out.

Because only discharge at long (annual) time scales is considered in this report, the computed discharge uncertainty computation can be simplified further (fig. 16; appendix 2, slide 44). Over and others (2004) analyzed the effect of the three uncertainty components considered here at the Romeoville streamgage, which also was operated as an index-velocity station (with an AVM). They determined that for time scales of a month or more, the total uncertainty is negligibly different from the uncertainty computed from the IVR parameter uncertainty alone; nevertheless, in this study, for the OLS regression computation, the random error term is retained, because for that regression, it is well defined.

The computations were done by Monte Carlo simulation (appendix 2, slide 45). The IVR regression parameters a and b were sampled from their joint Gaussian distribution characterized by the regression parameters listed in tables 8 and 9 (appendix 2, slides 37 and 38; intercept, slope, intercept SE, slope SE, and the correlation of the slope and intercept). For the simulations using the OLS regression parameters, the random error terms were modeled as a temporally independent mean zero Gaussian sequence with standard deviations noted on slide 45 in appendix 2. Because the stage and velocity unit-value data were available at 1- or 10-minute intervals and the median ADCP (discharge) measurement duration was 831 seconds (or about 14 minutes), a computation time step of 10 minutes was selected, and the unit-value stage and velocity data that were not already at that time interval were averaged over regular 10-minute intervals. The 10-minute stage and velocity were used with the appropriate stage-area rating curve and simulated IVR regression parameters to predict the discharge at each 10-minute interval, to which the random error was added in the case of OLS regression. These 10-minute discharge values were subsequently averaged over each day, and then at the daily time step. If less than one-half of the 10-minute values were available, the value for that day was filled with an independently simulated daily mean value using the other index-velocity meter if it had at least a half day of 10-minute values. Repeating this process 100 times for each index-velocity meter gave a simulation of the distribution of daily discharge values corresponding to the uncertainty of the IVR regression parameters as modeled by their joint distribution. These 100 simulations were finally averaged over water years. Unit-value velocity from the ADVM for WYs 2008–16 and for WYs 2006–15 from the AVM were mostly complete, and these ranges of water years were simulated for the ADVM and AVM, respectively.

Summary statistics (means of annual means, means of annual standard deviations, and means of annual coefficients of variation [CVs] of daily discharges) that describe the Monte Carlo simulation results for the ADVM and AVM regressions are listed in tables 12 and 13 (appendix 2, slides 46 and 48), respectively. Graphical depictions of the OLS regression results for the ADVM and AVM velocities are shown in figures 17 and 18 (appendix 2, slides 47 and 49), respectively. The means of annual means and the means of the standard deviations of annual means indicate the overall mean annual prediction and its uncertainty; the means of the daily CVs give indication of the range of values at the daily time scale. The standard deviations of the means of the annual means and the standard deviations of the daily CVs are provided to document the sampling variability of these statistics: if the number of simulations run were increased, these standard deviations would decrease as $1/\sqrt{n}$, where n is the number of

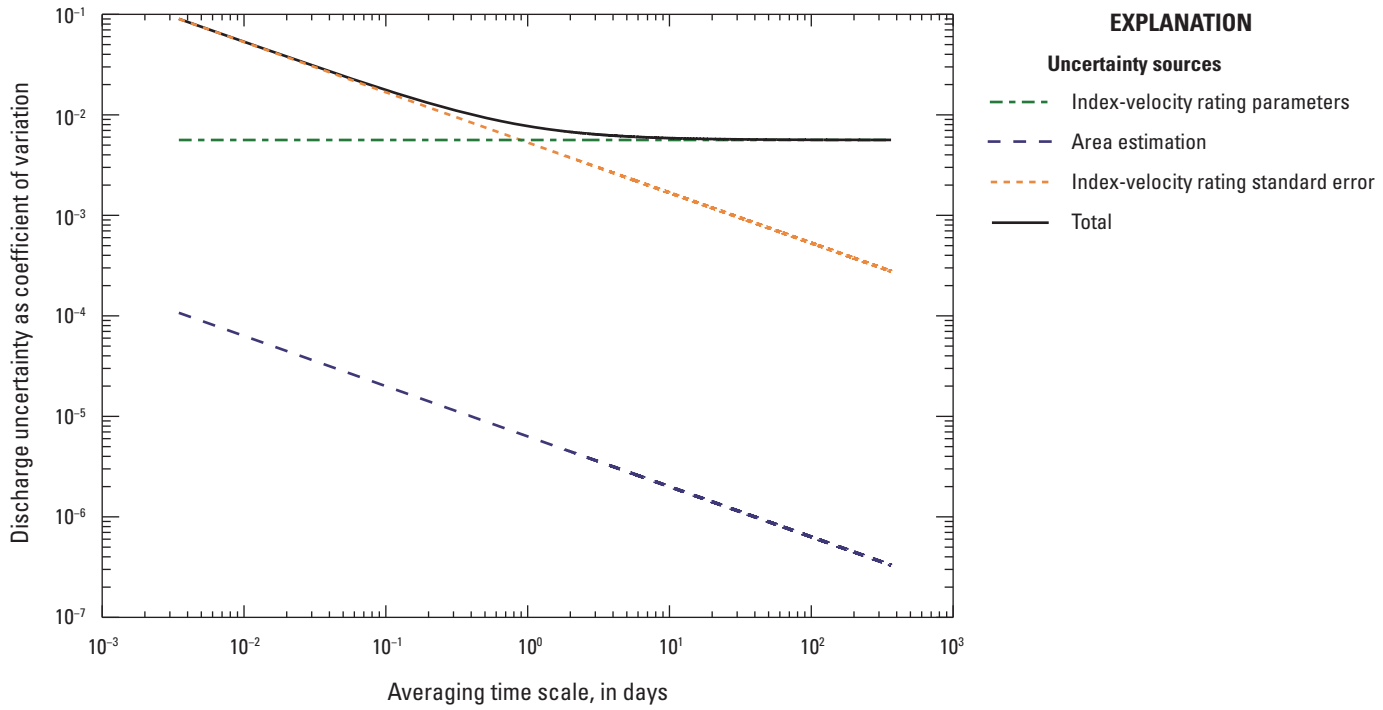

Figure 16. Effect of time scale of averaging on computed discharge uncertainty at U.S. Geological Survey streamgage 05536995, Chicago Ship and Sanitary Canal at Romeoville, Illinois (modified from Over and others, 2004).

simulations, but they are already small relative to the mean statistics themselves, so the use of 100 simulations is deemed to be sufficient.

In the ADVM results (table 12 and fig. 17; appendix 2, slides 46–47), the means of the annual means of the alternative regression methods are all somewhat less than those of the OLS regressions (as much as about 65 ft^3/s [about 2.4 percent] for the types of GLS regression with more extensive correlations [those with ADCP measurement error correlations of 0.1], and as little as about 20 ft^3/s [about 0.008 percent] for the types of EIV regression). This reduction in the predicted mean is inconsistent with the usually positive bias obtained when repredicting the fitting data (table 10; appendix 2, slide 39) and likely arises from the somewhat different distribution of velocity values used in the prediction as opposed to the fitting data (table 6 and fig. 11*A*, *B*; appendix 2, slide 29). Excepting the GLS regression with the extensive correlations, the means of the standard deviations of annual means of the alternative regressions are all substantially less than those from OLS regression when the predicted ADCP and ADVM errors are used but become relatively close to the OLS value (within about 3 ft^3/s or about 15 percent) when the specified uncertainties are doubled. The increase in the mean of the daily CVs relative to that of the OLS regression is about the same for all the alternative regressions at about 5 percent and is in qualitative agreement with the variance ratio increases observed among the alternative regressions when repredicting the fitting data (table 10; appendix 2, slide 39). If the OLS predictions are taken as the preferred set, the mean annual uncertainty of the annual means determined by this analysis is 21.2 ft^3/s when measured by the standard deviation, which is 0.8 percent of the mean.

The AVM results (table 13 and fig. 18; appendix 2, slides 48–49) are qualitatively similar to the ADVM results: the annual means of the alternative regressions are smaller than those of the OLS regression predictions, their annual standard deviations are much smaller when regressing using the predicted errors but similar when the errors are adjusted (by a factor of 3) excepting the GLS regression with the more extensive correlations (those with ADCP measurement error correlations of 0.1), and their daily CVs are larger. The mean uncertainty of the annual means for OLS regression is 34.5 ft^3/s when measured by the standard deviation (1.2 percent of the mean), compared to 21.2 ft^3/s and 0.8 percent, respectively, for the ADVM; the increase results from the larger uncertainties of the AVM OLS regression parameters. These values are also somewhat larger than the OLS regression-based estimate of 0.6 determined by Duncker and others (2006) for the AVM at the Romeoville streamgage when the ADCP was assumed to be without bias, as was assumed here. The mean biases of the alternative methods obtained when repredicting the fitting data (table 11; appendix 2, slide 40) are all negative, so the reduction in means in the predicted discharges qualitatively agrees, but the magnitudes are larger than the values in table 11 (appendix 2, slide 40) would indicate. For example, the mean bias of the EIV reprediction in table 11 (appendix 2, slide 40) is −0.0057 ft/s, which is 0.6 percent of the 0.945 ft/s mean of the ADCP velocity data

Table 12. Uncertainty statistics for annual mean (water years 2008–16) computed discharge for acoustic Doppler velocity meter-based index-velocity ratings for selected regression methods and error specifications.

[Computed at a 10-minute time step with 100 Monte Carlo samples. On average, 6.3 days per year were filled with acoustic velocity meter-based computed discharge, when available; on average, 1 day per year remains missing. IV, index velocity; ADCP, acoustic Doppler current profiler; ±, plus or minus; stdev, standard deviation; ft^3/s, cubic foot per second; CV, coefficient of variation; OLS, ordinary least squares; WLS, weighted least squares; GMR, Gauss-Markov regression; GLS, generalized least squares; GDR, generalized distance regression; EIV, errors in variables]

Regression method	Are errors specified?	Are IV errors considered?	Correlation of ADCP errors	Mean of annual means ± stdev(mean) (ft^3/s)	Mean of annual stdevs (ft^3/s)	Mean of daily CVs ± stdev(CVs)
OLS	No	No	None	2,660±2	21.2	0.595±0.0007
WLS	Yes	No	None	2,625±1	9.5	0.621±0.0003
WLS	[1]Yes × 2	No	None	2,625±2	18.1	0.620±0.0005
GMR (GLS)	Yes	No	[2]sel. corr.=0.5	2,622±1	12.2	0.625±0.0003
GMR (GLS)	[1]Yes × 2	No	[2]sel. corr.=0.5	2,619±2	18.0	0.626±0.0006
GMR (GLS)	Yes	No	[3]corr.=0.1	2,593±2	19.5	0.623±0.0003
GMR (GLS)	[1]Yes × 2	No	[3]corr.=0.1	2,596±3	33.4	0.623±0.0006
GDR (EIV)	Yes	Yes	None	2,638±1	12.9	0.621±0.0003
GDR (EIV)	[1]Yes × 2	Yes	None	2,640±2	22.2	0.623±0.0008

[1]"× 2" indicates that the estimated standard errors, both ACDP and IV, were multiplied by 2.

[2]As denoted by "sel.corr.=0.5," errors of ADCP (y-axis) measurements in immediate succession were assigned correlations of 0.5.

[3]As denoted by "corr.=0.1," errors of all ADCP (y-axis) measurements were assigned correlations of 0.1.

Table 13. Uncertainty statistics for annual mean (water years 2006–15) computed discharge for acoustic velocity meter-based index-velocity ratings for selected regression methods and error specifications.

[Computed at a 10-minute time step with 100 Monte Carlo samples. On average, 9.1 days per year were filled with acoustic Doppler velocity meter-based computed discharge, when available; on average, 1.2 days per year remain unfilled. IV, index velocity; ADCP, acoustic Doppler current profiler; ±, plus or minus; stdev, standard deviation; ft^3/s, cubic foot per second; CV, coefficient of variation; OLS, ordinary least squares; WLS, weighted least squares; GMR, Gauss-Markov regression; GLS, generalized least squares; GDR, generalized distance regression; EIV, errors in variables]

Regression method	Are errors specified?	Are IV errors considered?	Correlation of ADCP errors	Mean of annual means ± stdev(mean) (ft^3/s)	Mean of annual stdevs (ft^3/s)	Mean of daily CVs ± stdev(CVs)
OLS	No	No	None	2,834±3	34.5	0.545±0.0009
WLS	Yes	No	None	2,756±1	8.9	0.568±0.0002
WLS	[1]Yes × 3	No	None	2,755±3	28.7	0.566±0.0006
GMR (GLS)	Yes	No	[2]sel. corr.=0.5	2,742±1	12.1	0.575±0.0002
GMR (GLS)	[1]Yes × 3	No	[2]sel. corr.=0.5	2,750±3	33.4	0.572±0.0007
GMR (GLS)	Yes	No	[3]corr.=0.1	2,643±2	18.2	0.575±0.0002
GMR (GLS)	[1]Yes × 3	No	[3]corr.=0.1	2,646±6	57.6	0.575±0.0007
GDR (EIV)	Yes	Yes	None	2,784±1	11.9	0.570±0.0003
GDR (EIV)	[1]Yes × 3	Yes	None	2,786±3	32.2	0.571±0.0008

[1]"× 3" indicates that the estimated standard errors, both ACDP and IV, were multiplied by 3.

[2]As denoted by "sel.corr.=0.5," errors of ADCP (y-axis) measurements in immediate succession were assigned correlations of 0.5.

[3]As denoted by "corr.=0.1," errors of all ADCP (y-axis) measurements were assigned correlations of 0.1.

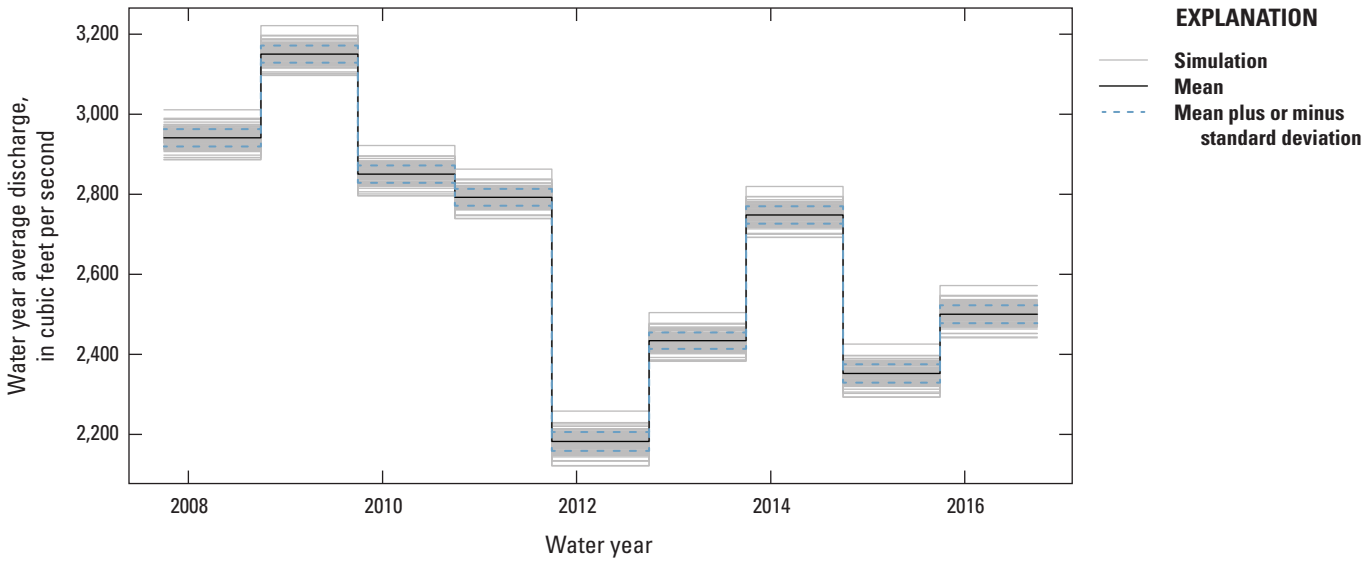

Figure 17. Ordinary least squares regression parameter uncertainty-based Monte Carlo results for computed discharge using acoustic Doppler velocity meter velocities.

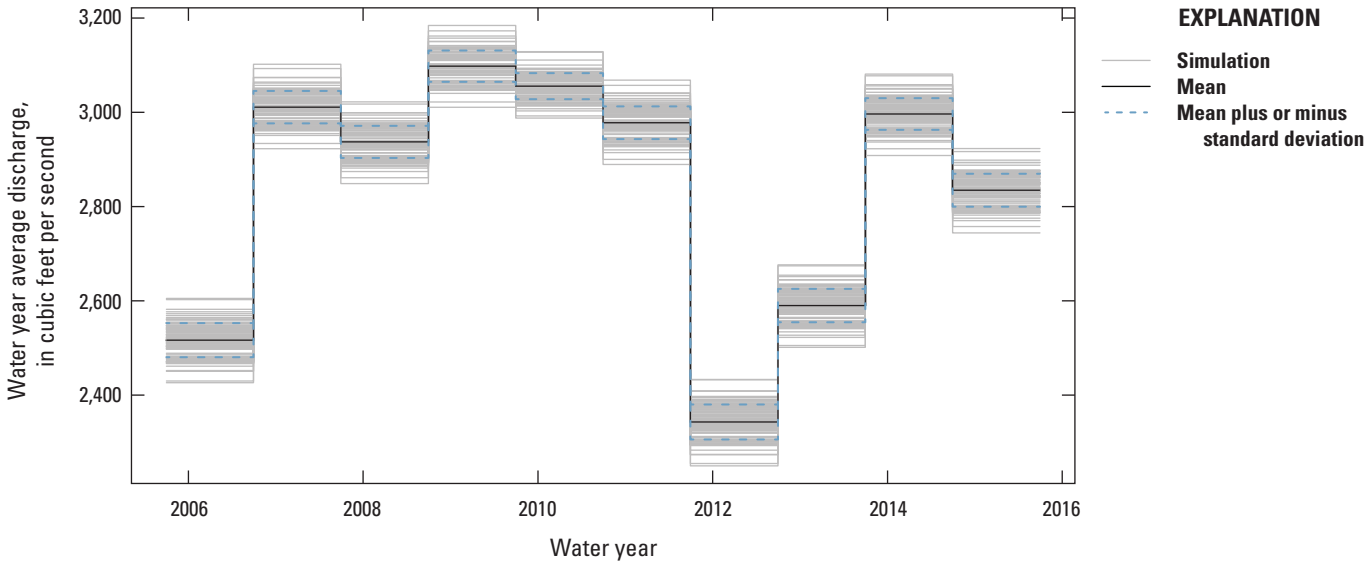

Figure 18. Ordinary least squares regression parameter uncertainty-based Monte Carlo results for computed discharge using acoustic velocity meter velocities.

used in AVM fitting data, whereas the corresponding reduction in the mean of annual means here is about 1.7 percent. As with the ADVM results, this difference likely results from the difference in velocity distribution between fitting and prediction datasets (table 6 and fig. 11*A*, *B*; appendix 2, slide 29). It may be possible to address this apparent effect of the differences in the fitting and prediction datasets by adjusting the distributions of the fitting datasets to better match those of the prediction datasets. If such an adjustment were done by subsampling, the uncertainty of the regression would increase at least somewhat; to avoid this effect, additional measurements could be made instead, if feasible.

Although OLS regression gives unbiased predictions when various conditions are met (the first four assumptions in table 5 [appendix 2, slide 28]), three problems are possible with using OLS regression for prediction in this context: (1) the OLS parameters (intercept and slope) are biased when the uncertainties are heteroscedastic; (2) the OLS parameters also are biased when there are errors in the x-axis variable; and (3) the variance of its predictions is biased low except when R^2 is 1. However, the heteroscedasticity of the residuals was observed to be mild (fig. 14*A*, *B*; appendix 2, slide 35) and the R^2 values are quite close to 1. Further, the biases in parameter values resulting from errors in the x-axis variable do not lead to biases in prediction when prediction is made using data with the same errors as used in the regression fitting and the distribution of the fitted data matches that of the predicted data. The first of these conditions is clearly met here, but some modest differences in distribution between the fitting and prediction data were noted. Although a strategy for addressing the differences in distribution was suggested, because those differences seem to be modest, the OLS regression predictions seem to be the best among the available methods and are expected to be reliable if not exact. Making use of one of the alternative approaches, such as one based on EIV regression with specified errors, would require developing more confidence in the accuracy of the specified errors.

Summary

Measurement and computed discharge uncertainties are especially important for the Chicago Sanitary and Ship Canal near Lemont, Illinois, streamgage (U.S. Geological Survey station 05536890) because of its critical role in the Lake Michigan Diversion Accounting done by the U.S. Army Corps of Engineers. Discharge at the streamgage is computed based on an index-velocity rating (IVR), computed by linear regression, that uses a continuous velocity meter for the predictor and velocities computed from discharge measurements by an acoustic Doppler current profiler (ADCP) as the predictand. During most of the study period (water years 2006–16), two index-velocity meters were in use at the site, an acoustic velocity meter (AVM) and an acoustic Doppler velocity meter (ADVM). Type B (nonempirical) uncertainties were estimated using the first-order second moment approach with Gaussian elemental uncertainties for the AVM and ADVM index-velocity meter deployments, and for the water-level (stage) measurements by pressure transducer, at the streamgage. The AVM and ADVM velocity uncertainties, expressed as standard deviations, were predicted to be Gaussian and similar in magnitude: about 2.5 percent of velocity except near zero velocity where the ADVM uncertainty was predicted to be about 0.009 foot per second (ft/s) and the AVM uncertainty about 0.003 ft/s. The stage uncertainty was estimated to be about 0.027 foot, independent of water level. Uncertainty of the ADCP measurements was estimated using the part-judgment, part-empirical method built into the ADCP measurement processing software QRev. The ADCP uncertainties, converted to mean channel velocities, were predicted to be larger than those of the index-velocity meters, having a lower bound of 2.5 percent of velocity but sometimes having much larger fractions of velocity, especially at lower values of velocity.

The predicted uncertainties were compared to the results from fitting ADVM and AVM-based IVRs using different types of linear regressions. These composed ordinary least squares (OLS) regression, which is the U.S. Geological Survey standard method for IVRs, and alternative methods that make use of specified uncertainties of the regression data, including weighted least squares and errors-in-variables regressions, which allow specification of errors on the y axis and on both the x and y axes, respectively. The IVRs fitted using OLS regression were found to be linear with coefficient of determination values of at least 0.988. The standard error of the residuals of the AVM OLS regression (0.104 ft/s) was about twice as large as those from the ADVM (0.056 ft/s); the growth of the residuals with velocity was modest, unlike the predicted AVM and ADVM uncertainties, and the distributions of the residuals, although symmetric around zero, had fatter tails than predicted by a Gaussian distribution. AVM and ADVM residuals from common measurements were modestly positively correlated, indicating contributions from both index-velocity and ADCP errors.

For the regressions where the uncertainties were specified, the chi-squared test indicated that the probability that the specified uncertainties were of the correct magnitude was negligibly small. The test was satisfied only when the specified uncertainties were multiplied by about 2 and 3 for the ADVM and AVM uncertainties, respectively; therefore, from multiple perspectives, the regression analyses indicate that the index velocity uncertainties estimated from the type B approach and the ADCP uncertainties estimated using QRev, when taken together, do not agree with the empirical data.

The fitted IVRs were then used to compute discharge and its uncertainty using Monte Carlo sampling of the estimated joint distribution of the IVR parameters. From the OLS regression IVR, at the annual time scale, which is of primary interest to the Lake Michigan Diversion Accounting process, the mean uncertainty of annual mean discharge measured by the coefficient of variation was determined to be about 0.8 percent based on the ADVM velocities and about 1.2 percent based on

the AVM velocities. The alternative regression methods with specified uncertainties gave similar uncertainty predictions when the specified uncertainties were increased by the same factors as were used to satisfy statistical testing in the regression fitting. However, the alternative regressions predicted somewhat smaller mean discharges and larger variability at the daily time scale. Various assumptions need to be met for OLS predictions to be unbiased in mean and variance in the presence of heteroscedastic uncertainties and errors in the x-axis variable, but it was argued that these are all at least approximately met and therefore the discharge predictions based on the OLS regression results are expected to be reliable if not exact.

Several possible ways could be used to extend or improve upon the results reported here. The estimated ADVM and AVM uncertainties could be reconsidered to address the error components whose uncertainties were not estimated and to refine the estimated values. This reconsideration may be especially relevant in light of the relative magnitudes of the ADVM and AVM uncertainties and their strong dependence on velocity as compared to the index-velocity residuals. Because of the non-Gaussianity of the residuals, it may be informative to examine the measurements associated with the outliers among the residuals to look for anomalous flow or measurement conditions. The prediction of ADCP uncertainties continues to be an active area of research, and more accurate ADCP uncertainty estimates than were used here could become feasible. A statistical strategy was suggested that would address a weakness in the use of OLS regression for prediction (that of differences in the distribution of the fitting and prediction data). Further, it may be possible to find or develop a method that enables further information to be gleaned from the regression residuals, such as the ratio of errors on the x and y axes or their growth with velocity. By applying these strategies, it may be possible to further improve the accuracy of the computed discharge and its estimated uncertainty at this important streamgage.

References Cited

Buonaccorsi, J.P., 2010, Measurement error—Models, methods, and applications: New York, Chapman & Hall/CRC, 464 p.

Duncker, J.J. and Johnson, K.K., 2015, Hydrology of and current monitoring issues for the Chicago Area Waterway System, northeastern Illinois: U.S. Geological Survey Scientific Investigations Report 2015–5115, 48 p., accessed December 2016 at https://doi.org/10.3133/sir20155115.

Duncker, J.J., Over, T.M., and Gonzalez, J.A., 2006, Computation and error analysis of discharge for the Lake Michigan Diversion Project in Illinois—1997–99 water years: U.S. Geological Survey Scientific Investigations Report 2006–5018, 70 p., accessed March 2007 at https://doi.org/10.3133/sir20065018.

Espey, W.H., Barnes, H.H., and Vigander, S., 1981, Lake Michigan Diversion—Findings of the technical committee for review of diversion flow measurements and accounting procedures: U.S. Army Corps of Engineers, Chicago District, 110 p.

Espey, W.H., Clemmens, B., and Halverson, B., 2014, Lake Michigan Diversion—Findings of the seventh technical committee for review of diversion flow measurements and accounting procedures: U.S. Army Corps of Engineers, Chicago District, 124 p.

Espey, W.H., Melching, C., and Muste, M., 2009, Lake Michigan Diversion—Findings of the sixth technical committee for review of diversion flow measurements and accounting procedures: U.S. Army Corps of Engineers, Chicago District, 198 p.

Espey, W.H., Melching, C.S., and Muste, M., 2019, Lake Michigan Diversion Committee—Findings of the eighth technical committee for review of diversion flow measurements and accounting procedures: U.S. Army Corps of Engineers, Chicago District, 175 p.

Faraway, J.J., 2005, Linear models with R: New York, Chapman & Hall/CRC, 229 p.

Fuller, W.A., 1987, Measurement error models: New York, John Wiley & Sons, 440 p.

González-Castro, J.A., Buzard, J., and Mohamed, A., 2016, RiverFlowUA—A package to estimate total uncertainty in ADCP discharge measurements by FOTSE—With an application in hydrometry, *in* Constantinescu, G., Garcia, M., and Hanes, D., eds., River Flow 2016—Proceedings of the International Conference on Fluvial Hydraulics, St. Louis, Missouri, July 11–14, 2016: London, Taylor & Francis Group, p. 715–723.

González-Castro, J.A., and Mohamed, A., 2007, Uncertainty assessment of a stage-based flow rating accounting for uncertainties in both dependent and independent variables, *in* Cowen, E.A., Hill, D., George, C., Jirka, G., Muste, M., Admiraal, D.M., Blake, A., Frizell, W., Nakato, T., Oberg, K., Pugh, C., Rehmann, C., Rennie, C., Schmidt, A.R. Styles, S., Vermeyen, T., Wahl, T. and Zhu, D., eds., Book of extended abstracts of the Hydraulic Measurement & Experimental Methods Conference 2007, Lake Placid, New York, September 10–12, 2007 [Conference paper]: Reston, Va., Environmental & Water Resources Institute of the American Society of Civil Engineers and the International Association of Hydraulic Engineering and Research, p. 53–58.

González-Castro, J.A., and Muste, M., 2007, Framework for estimating uncertainty of ADCP measurements from a moving boat by standardized uncertainty analysis: Journal of Hydraulic Engineering (New York, N.Y.), v. 133, no. 12, p. 1390–1410. [Also available at https://doi.org/10.1061/(ASCE)0733-9429(2007)133:12(1390).]

Helsel, D.R., Hirsch, R.M., Ryberg, K.R., Archfield, S.A., and Gilroy, E.J., 2020, Statistical methods in water resources: U.S. Geological Survey Techniques and Methods, book 4, chap. A3, 458 p. [Also available at https://doi.org/10.3133/tm4A3.]

Hirsch, R.M., 1982, A comparison of four streamflow record extension techniques: Water Resources Research, v. 18, no. 4, p. 1081–1088. [Also available at https://doi.org/10.1029/WR018i004p01081.]

Horner, I., Renard, B., Le Coz, J., Branger, F., McMillan, H.K., and Pierrefeu, G., 2018, Impact of stage measurement errors on streamflow uncertainty: Water Resources Research, v. 54, no. 3, p. 1952–1976. [Also available at https://doi.org/10.1002/2017WR022039.]

Huang, H., 2018, Estimating uncertainty of streamflow measurements with moving-boat acoustic Doppler current profilers: Hydrological Sciences Journal, v. 63, no. 3, p. 353–368. [Also available at https://doi.org/10.1080/02626667.2018.1433833.]

Illinois Environmental Protection Agency, [2021], Lake Michigan, Illinois Environmental Protection Agency web page, accessed August 2021 at https://www2.illinois.gov/epa/topics/water-quality/monitoring/Pages/lake-michigan.aspx.

International Organization for Standardization, 2010, Determination and use of straight-line calibration functions: ISO Technical Standard 28037, 63 p.

Jackson, P.R., 2018, Characterizing variability in vertical profiles of streamwise velocity and implications for streamgaging practices in the Chicago Sanitary and Ship Canal near Lemont, Illinois, January 2014 to July 2017: U.S. Geological Survey Scientific Investigations Report 2018–5128, 73 p., accessed November 2018 at https://doi.org/10.3133/sir20185128.

Jackson, P.R., Johnson, K.K., and Duncker, J.J., 2012, Comparison of index velocity measurements made with a horizontal acoustic Doppler current profiler and a three-path acoustic velocity meter for computation of discharge in the Chicago Sanitary and Ship Canal near Lemont, Illinois: U.S. Geological Survey Scientific Investigations Report 2011–5205, 42 p., accessed September 2013 at https://doi.org/10.3133/sir20115205.

Johnson, K.K., Duncker, J.J., and Jackson, P.R., 2012, The role of the U.S. Geological Survey in Lake Michigan Diversion Accounting in Illinois, 1984–2010: U.S. Geological Survey Open-File Report 2012–1243, 73 p., accessed June 2017 at https://doi.org/10.3133/ofr20121243.

Joint Committee for Guides in Metrology, 2008, Evaluation of measurement data—Guide to the expression of uncertainty in measurement: Bureau International des Poids et Mesures report JCGM 100:2008, 120 p. [Also available at: https://www.bipm.org/documents/20126/2071204/JCGM_100_2008_E.pdf/cb0ef43f-baa5-11cf-3f85-4dcd86f77bd6.]

Kim, B., Lee, T., and Ouarda, T.B.M.J., 2014, Total least square method applied to rating curves: Hydrological Processes, v. 28, no. 13, p. 4057–4066. [Also available at https://doi.org/10.1002/hyp.9944.]

Laenen, A., 1985, Acoustic velocity meter systems: U.S. Geological Survey Techniques of Water-Resources Investigations, book 3, chapter A17, 38 p. [Also available at https://doi.org/10.3133/twri03A17.]

Le Coz, J., Pierrefeu, G., and Paquier, A., 2008, Evaluation of river discharges monitored by a fixed side-looking Doppler profiler: Water Resources Research, v. 44, no. 4, art. W00D09, 13 p., accessed March 2021 at https://doi.org/10.1029/2008WR006967.

Levesque, V.A., and Oberg, K.A., 2012, Computing discharge using the index velocity method: U.S. Geological Survey Techniques and Methods, book 3, chapter A23, 148 p., accessed May 2015 at https://doi.org/10.3133/tm3A23.

Moore, S.A., Jamieson, E.C., Rainville, F., Rennie, C.D., and Mueller, D.S., 2017, Monte Carlo approach for uncertainty analysis of acoustic Doppler current profiler discharge measurement by moving boat: Journal of Hydraulic Engineering (New York, N.Y.), v. 143, no. 3, art. 04016088, 15 p., accessed July 2020 at https://doi.org/10.1061/(ASCE)HY.1943-7900.0001249.

Morlock, S.E., Nguyen, H.T., and Ross, J.H., 2002, Feasibility of acoustic Doppler velocity meters for the production of discharge records from U.S. Geological Survey streamflow-gaging stations: U.S. Geological Survey Water-Resources Investigations Report 2001–4157, 56 p. [Also available at https://doi.org/10.3133/wri20014157.]

Mueller, D.S., 2016, QRev—Software for computation and quality assurance of acoustic Doppler current profiler moving-boat streamflow measurements—Technical manual for version 2.8: U.S. Geological Survey Open-File Report 2016–1068, 79 p., accessed October 2020 at https://doi.org/10.3133/ofr20161068.

National Physical Laboratory, 2010, Software to support ISO/TS 28037:2010E: National Physical Laboratory software release, accessed December 14, 2016, at https://www.npl.co.uk/resources/software/iso-ts-28037-2010e.

Naudet, G., Pierrefeu, G., Berthet, T., Triol, T., Delamarre, K., and Blanquart, B., 2019, OURSIN—OUtil de Répartition deS INcertitudes de mesure de débit par aDcp mobile: Houille Blanche, v. 105, no. 3–4, p. 93–101. [OURSIN—Uncertainty distribution tool for moving-boat aDcp measurements] [In French] [Also available at https://doi.org/10.1051/lhb/2019056.]

Over, T.M., Duncker, J.J., and Gonzalez-Castro, J.A., 2004, Comparison of estimates of uncertainty of discharge at U.S. Geological Survey index-velocity gages on the Chicago Sanitary and Ship Canal, Illinois, *in* Sehlke, G., Hayes, D.F., and Stevens, D.K., eds., Critical Transactions in Water and Environmental Resources Management—Proceedings of the 2004 World Water and Environmental Resources Congress, Salt Lake City, Utah, June 27–July 1, 2004 [Conference paper]: Reston, Va., American Society of Civil Engineers, p. 2342–2352. [Also available at https://doi.org/10.1061/40737(2004)288.]

Over, T.M., Muste, M., Duncker, J.J., Tsai, H.-W., Jackson, P.R., Johnson, K.K., Engel, F.L., and Prater, C.D., 2017, Uncertainty analysis of an index velocity meter and discharge computations at the Chicago Sanitary and Ship Canal near Lemont, Illinois, *in* Proceedings of the Hydraulic Measurements and Experimental Methods Conference, Durham, New Hampshire, July 9–12, 2017 [Conference paper]: Environmental & Water Resources Institute of the American Society of Civil Engineers, 6 p.

Prater, C.D., LeRoy, J.Z., Engel, F.L., and Johnson, K.K., 2021, Discharge measurements at U.S. Geological Survey streamgage 05536890 Chicago Sanitary and Ship Canal near Lemont, Illinois, 2005–2013: U.S. Geological Survey data release, accessed March 2021 at https://doi.org/10.5066/F7X63K41.

Press, W.H., Teukolsky, S.A., Vetterling, W.T., and Flannery, B.P., 1992, Numerical recipes in Fortran 77—The art of scientific computing (2d ed.): New York, Cambridge University Press, 973 p.

Qualisyst Ltd., 2015, QMSys GUM Enterprise, version 4.10: Qualisyst Ltd., software release, accessed August 15, 2015, at http://www.qsyst.com/qualisyst_en.htm.

R Core Team, 2019, R—A language and environment for statistical computing, version 4.0.4 (Lost Library Book): R Foundation for Statistical Computing software release, accessed February 25, 2021, at https://www.R-project.org/.

Sauer, V.B., and Turnipseed, D.P., 2010, Stage measurement at gaging stations: U.S. Geological Survey Techniques and Methods book 3, chapter A7, 45 p., accessed December 2017 at https://doi.org/10.3133/tm3A7.

U.S. Geological Survey, 1996, Policy concerning accuracy of stage data: U.S. Geological Survey Office of Surface Water Technical Memorandum no. 96.05, accessed January 16, 2022, at https://water.usgs.gov/water-resources/memos/memo.php?id=945.

U.S. Geological Survey, 2021, USGS water data for the Nation: U.S. Geological Survey National Water Information System database, accessed May 5, 2021, at https://doi.org/10.5066/F7P55KJN.

Zhang, L., Mohamed, A., and González-Castro, J.A., 2012, Uncertainties in flow discharge rating by generalized least squares method, *in* Admiraal, D.M., and Hill, D.F., eds., Proceedings of the Hydraulic Measurement & Experimental Methods Conference 2012, Snowbird, Utah, August 12–15, 2012 [Conference paper]: American Society of Civil Engineers/Environmental and Water Resources Institute, 6 p.

Appendix 1. Slide Descriptions

The slides that are referenced throughout the main report are available for download in appendix 2. Descriptions of each slide, and the headings that correspond to the slide callouts in the main report, are included in appendix 1 for the convenience of the reader.

1. Title slide.

Introduction

2. Background and history on the Lake Michigan diversion and the Lake Michigan Diversion Accounting program.
3. Map of the Chicago Sanitary and Ship Canal and related features of the Chicago Area Waterway System.
4. History of streamgaging by the U.S. Geological Survey for the Lake Michigan Diversion Accounting program.
5. Photographs of the gage house and the instrumentation near it and the Chicago Sanitary and Ship Canal upstream from the Chicago Sanitary and Ship Canal near Lemont, Illinois, streamgage.
6. Plan view of the Chicago Sanitary and Ship Canal near Lemont streamgage (from Jackson and others, 2012).
7. List of instrumentation at the Chicago Sanitary and Ship Canal near Lemont streamgage.
8. Schematics of the acoustic velocity meter (AVM) and acoustic Doppler velocity meter (ADVM) deployments at the Chicago Sanitary and Ship Canal near Lemont streamgage (from Jackson and others, 2012).
9. The four steps of the approach to uncertainty estimation presented in this report.
10. Description of the dataset of paired acoustic Doppler current profiler (ADCP) and index-velocity meter (AVM and ADVM) measurements used to fit rating curves in this report.

Estimation of Measurement Uncertainty for Continuous Sensors

11. Title slide of the section presenting the first step with general information about the methods.
12. Description of error propagation by the first-order second moment method.
13. Data reduction equation (DRE) for AVM uncertainty.
14. Expanded DRE as entered into the QMSys error propagation software.
15. Elemental uncertainty values for AVM measurements.
16. Illustration of the graphical output of the QMSys software for AVM uncertainty analysis.
17. DRE for ADVM uncertainty, basic and as entered into QMSys.
18. Elemental uncertainty values for ADVM measurements.
19. Plot of ADVM and AVM uncertainty as a function of velocity, with discussion.
20. DRE for water-level (stage) measurement uncertainty as entered into QMSys.
21. Elemental uncertainty values (and total uncertainty) for stage measurements.

Estimation of Measurement Uncertainty of Discharge Measurements

22. Title slide of section with background information regarding methodology applied.
23. Table detailing components of ADCP measurement uncertainty estimation with QRev giving method of computation and range and median of results.
24. Plot of predicted ADCP measurement uncertainties as a function of velocity with discussion.

Determination of Index-Velocity Ratings

25. Title slide of section.
26. Discussion of fitting of index-velocity ratings (IVRs) in U.S. Geological Survey practice.
27. Presentation and discussion of the stage-area ratings corresponding to the AVM and ADVM measurements.

28. Assumptions of ordinary least squares (OLS) regression and their implications for uses for the regression results.

29. Comparison of the probability distributions of the ADVM and AVM velocity data used for fitting the IVRs with those used for prediction.

30. Table of the regression methods considered in this study and their properties.

31. The two software packages used for fitting IVRs in the analysis presented in this report.

32. Background and implications of chi-squared testing of regression model fits.

33. Scatterplots of OLS regression fits of ADVM and AVM-based IVRs using data common to both index-velocity meters.

34. Gaussian quantile-quantile plots of the residuals of the OLS regression fits of ADVM and AVM-based IVRs using data common to both index-velocity meters, portraying the degree to which the residuals fit a Gaussian distribution.

35. Plots of square roots of the absolute standardized residuals versus fitted values with fitted local polynomial regression (loess) line indicating trends in the variability of the residuals.

36. Scatterplot and correlation values of residuals of AVM and ADVM-based IVRs using data common to both index-velocity meters.

37. Table of fitting statistics of ADVM-based IVRs for OLS and selected alternative regression models.

38. Table of fitting statistics of AVM-based IVRs for OLS and selected alternative regression models.

39. Table of prediction statistics of ADVM-based IVRs for OLS and selected alternative regression models for prediction of the values used in the regression fitting.

40. Table of prediction statistics of AVM-based IVRs for OLS and selected alternative regression models for prediction of the values used in the regression fitting.

Computation of Discharge and its Uncertainty

41. Title slide of section.

42. Description of use of IVRs—and stage-area ratings—for computation of discharge.

43. Description of sources of uncertainty in discharge computed using IVRs.

44. Discussion of the effect of the time scale of averaging on the magnitudes of contributions of uncertainty sources contributing to the uncertainty of computed discharge.

45. Description of how computed discharge uncertainty was computed in this study.

46. Table of results of computed discharge using the ADVM-based IVRs for selected regression methods.

47. Plot of annual mean discharge from simulations of ADVM-based IVR for OLS regression.

48. Table of results of computed discharge using the AVM-based IVRs for selected regression methods.

49. Plot of annual mean discharge from simulations of AVM-based IVR for OLS regression.

Summary

50. Summary of results regarding predicted measurement uncertainties.

51. Summary of results regarding IVRs based on OLS regression.

52. Summary of results regarding IVRs based on alternative regression methods.

53. Summary of results regarding prediction of discharge and its uncertainty.

54. Final remarks.

55. References cited—page 1.

56. References cited—page 2.

Appendix 2. Slides

The slides mentioned throughout the main report are available for download from https://doi.org/10.3133/ofr20221007.

For more information about this publication, contact:
Director, USGS Central Midwest Water Science Center
405 North Goodwin Ave.
Urbana, IL 61801
217–328–8747

For additional information, visit: https://www.usgs.gov/centers/cm-water

Publishing support provided by the
Rolla Publishing Service Center

ISSN 2331-1258 (online)
https://doi.org/10.3133/ofr20221007